Submitted to *Mass Spectrom. Rev.*

Periodic Trends in the Hydration Energies and Critical Sizes of Alkaline Earth and Transition Metal Dication Water Complexes

Fan Yang and P. B. Armentrout*

Department of Chemistry, University of Utah, 315 S. 1400 E. Rm 2020, Salt Lake City, UT 84112

*To whom correspondence should be addressed.

Email: armentrout@chem.utah.edu

Phone: (801) 581-7885

Short title: Periodic trends in hydration energies

Keywords: bond dissociation energies, guided ion beam tandem mass spectrometry, kinetic energy dependence, thermodynamics

Table of Contents

ABSTRACT

This review encompasses guided ion beam tandem mass spectrometry studies of hydrated metal dication complexes. Metals include the Group 2 alkaline earths (Mg, Ca, Sr, and Ba), late first-row transition metals (Mn, Fe, Co, Ni, Cu, and Zn), along with Cd. In all cases, threshold collision induced dissociation experiments are used to quantitatively determine the sequential hydration energies for $M^{2+}(H_2O)_x$ complexes ranging in size from one to eleven water molecules. Periodic trends in these bond dissociation energies are examined and discussed. Values are compared to other experimental results when available. In addition to dissociation by simple water ligand loss, complexes at a select size (which differs from metal to metal) are also observed to undergo charge separation to yield a hydrated metal hydroxide cation and a hydrated proton. This leads to the concept of a critical size, x_{crit}, and the periodic trends in this value are also discussed.

I. INTRODUCTION

An understanding of solvation phenomena has long been a goal of many gas-phase studies. Quantitative characterization of solvation thermodynamics can potentially permit the extrapolation of detailed information available in gas-phase work to the condensed phase. Water is arguably the most important solvent such that hydration studies are foremost among this work. Interactions of metals in water are keys to understanding physiological and environmental chemistry. Delivery of metal nutrients to enzymes involves hydrated metal cations and the systematic removal of the inner hydration sphere in order to allow the metal to bind to the enzymatic site. Likewise, remediation efforts can be achieved by isolation of metal cations using selective coordination with ligands that replace the hydration sphere. Thus, the thermodynamics of the inner hydration shell are of broad interest and utility.

For these reasons, the thermodynamics of gas-phase metal dication-water complexes, $M^{2+}(H_2O)_x$, have been studied extensively using ion equilibria,(Blades, et al., 1990;Blades, et al., 1990;Dzidic & Kebarle, 1970;Peschke, et al., 2000;Peschke, et al., 1999;Peschke, et al., 1998;Searles & Kebarle, 1969) blackbody infrared radiative dissociation (BIRD),(Donald, et al., 2011;Rodriguez-Cruz, et al., 1999;Rodriguez-Cruz, et al., 1999;Rodriguez-Cruz, et al., 1998) and collision-induced dissociation (CID).(Anderson, et al., 1995;Cheng, et al., 1992;Jayaweera, et al., 1990;Shvartsburg & Siu, 2001) Notably, because they are thermal techniques, neither ion equilibria nor BIRD studies are capable of measuring the most tightly bound inner shell water ligands and earlier CID studies were also limited in this regard. More advanced threshold CID (TCID) experiments and analysis tools developed in our group have extended such thermodynamic information to the inner shell ligands. Our TCID studies now include the Group 2 alkaline earth dications, where M = Mg,(Carl & Armentrout, 2013) Ca,(Carl & Armentrout, 2012;Carl, et al., 2007) Sr,(Carl, et al., 2010;Wheeler, et al., 2018) and Ba,(Wheeler, et al., 2015) and late 3d transition metal dications, where M = Mn,(Yang, et al.) Fe,(Hofstetter & Armentrout, 2013) Co,(Coates & Armentrout, 2018) Ni,(Coates & Armentrout, 2017) Cu,(Sweeney & Armentrout, 2014;Sweeney & Armentrout, 2015) and Zn,(Cooper & Armentrout, 2009;Cooper, et al., 2009)

along with M = Cd.(Cooper & Armentrout, 2011;Cooper & Armentrout, 2010) In all these studies, we examined the dissociation pathways and extracted quantitative bond dissociation energies (BDEs) for hydration, and coupled the experimental work with explorations of the ground structures (GSs) of the complexes using quantum chemical calculations (as validated by thermochemical comparisons). These metal dication studies supplement previous TCID work examining the hydration enthalpies of singly charged cations (H^+,(Dalleska, et al., 1993) Li^+,(Rodgers & Armentrout, 1997) Na^+, Mg^+, Al^+,(Dalleska, Tjelta, et al., 1994) Ti^+ – Cu^+,(Dalleska, Honma, et al., 1994;Schultz & Armentrout, 1993) $FeOH^+$,(Sander & Armentrout, 2019) $CoOH^+$,(Coates & Armentrout, 2017) $CuOH^+$,(Sweeney & Armentrout, 2014) Ag^+,(Koizumi, et al., 2003) $Th(OH)_3^+$(Kafle, et al., 2020)) which will not be detailed here.

In this review, we focus on the periodic trends in the alkaline earth and transition metal dication hydration energies. In all cases, TCID performed using a guided ion beam tandem mass spectrometer (GIBMS) was used to measure the threshold energies precisely and directly for water loss from the metal dication-water complexes. The dominant process observed in all studies was loss of a single water ligand, reaction (1),

$$M^{2+}(H_2O)_x \rightarrow M^{2+}(H_2O)_{x-1} + H_2O \quad (1)$$

followed by sequential loss of additional water molecules for $x > 1$. In all of these studies, $M^{2+}(H_2O)_x$ complexes at a specific value of x were also observed to dissociate into two singly-charged species, reaction (2), in a charge separation (CS) process that is competitive with the loss of water.

$$M^{2+}(H_2O)_x \rightarrow MOH^+(H_2O)_y + H^+(H_2O)_{x-y-1} \quad (2)$$

The products of such reactions will be referred to as y+(x-y-1) below. The observation of reaction (2) for the hydrated metal dication complexes leads to the concept of the critical size, x_{crit}, which was originally defined as "the maximum number of ligands at which dissociative charge transfer is competitive with simple ligand loss".(Shvartsburg & Siu, 2001) This definition results in ambiguities in the assignment of x_{crit} that depend on the experimental conditions. For example, Kebarle and coworkers determined the critical size of $Mn^{2+}(H_2O)_x$ to be 3,(Blades, et al.,

1990;Blades, et al., 1990;Jayaweera, et al., 1990) whereas Shvartzburg and Siu suggested the largest complex exhibiting CS occurred at x_{crit} = 4.(Shvartsburg & Siu, 2001) Such discrepancies occur because the extent of the competition between reactions (1) and (2) depends strongly on the experimental conditions and sensitivity. Further, in routine mass spectrometry experiments, there is nothing that couples the observation of the two singly-charged fragments of reaction (2) with each other or with a particular reactant ion. To overcome the disparity in such observations, we have previously suggested a more precise definition of the critical size for hydrated metal dications, i.e., the largest value of x at which charge separation is *energetically* favored over the loss of one water ligand.(Cooper, et al., 2009) Determination of this critical size therefore requires that the energetics of the competing dissociation reactions be evaluated, which can be performed using GIBMS or computationally. In our studies, the energy thresholds at 0 K for these competitive reactions are determined, thereby bypassing considerations associated with how the experimental conditions affect the competition, as described further below. The redefined x_{crit} has applied to all hydrated dication studies published by the Armentrout group, as discussed below.

As mentioned above, theoretical calculations were also performed to complement the experimental work. GSs for each metal dication-water complex along with low-lying isomers for each cluster size were obtained using theoretical calculations. This provides more complete information regarding how metal dications interact with water molecules. In addition, pathways for the CS reactions were mapped computationally along the reaction coordinate because this reaction must have a tight transition state (TS) associated with the Coulomb barrier generated upon approach of the two singly-charged products, designated as TS[y,x-y-1] below. Therefore, decomposition of the $M^{2+}(H_2O)_x$ complex via CS requires moving one or more water ligands into outer solvent shells, a rearrangement sequence that we have documented for several M^{2+}. This critical analysis provides an in depth understanding of the CS reactions because it more clearly defines the competition between water loss (over a loose TS) and CS reactions.

II. EXPERIMENTAL AND COMPUTATIONAL METHODS

A. Experimental Procedures. TCID experiments of hydrated metal dications were carried out using a homebuilt GIBMS, which has been described in detail previously.(Ervin & Armentrout, 1985;Muntean & Armentrout, 2001) Detailed conditions for each individual experiment are provided in the original publications. Hydrated metal dications, $M^{2+}(H_2O)_x$, were generated from low concentration (~10^{-4} M) solutions made of HPLC grade water and metal dication salts introduced into the vacuum chamber through an electrospray ionization (ESI) source. The ESI source(Moision & Armentrout, 2007) comprises an electrospray needle, a heated capillary, an 88-plate radio-frequency (rf) ion funnel,(Shaffer, et al., 1998) and a rf-only hexapole ion guide (6P). An in-source fragmentation (FINS) device, which places dc electrodes in between the rods of the hexapole, can be implemented to induce fragmentation to form smaller complex sizes than generated in the original ESI production.(Carl, et al., 2010;Carl, et al., 2009) After fragmentation, the ions were thermalized to 300 K in the hexapole region as they underwent ~10^4 collisions with ambient gas.(Carl & Armentrout, 2013;Carl, et al., 2010;Carl, et al., 2009;Carpenter, et al., 2017;Coates & Armentrout, 2017;Coates & Armentrout, 2018;Coates & Armentrout, 2017;Wheeler, et al., 2015;Ye & Armentrout, 2008) The ions were extracted from the ion source and focused into a magnetic sector momentum analyzer to mass select the desired $M^{2+}(H_2O)_x$ complex. The ions were then decelerated to a specific energy variable over several orders of magnitude and injected into a dual octopole ion guide.(Ervin & Armentrout, 1985;Gerlich, 1992;Muntean & Armentrout, 2001) A gas cell that surrounds part of the first octopole ion guide contained relatively low pressures of Xenon as a collision gas. The pressure was sufficiently low that single collision conditions predominate, although the pressure dependence of the results was explicitly checked to ensure single collision conditions.{Aristov, 1986 #23;Dalleska, Honma, 1994 #219;Hales, 1990 #289} After the collision cell, all ions drift to the end of the second octopole where they were extracted and focused into a quadrupole mass filter (QMF) for mass analysis. The unreacted precursor and product ions were collected using a Daly-type detector(Daly, 1960) and the signals processed using standard pulse counting techniques. Raw

experimental data were recorded as precursor and product ion intensities as a function of the laboratory voltage applied to the ions in the collision region.

B. Data analysis. The intensities of the reactant and product ions were converted to absolute reaction cross sections as described previously,(Ervin & Armentrout, 1985) with absolute uncertainties estimated at ±20%. The ions were accelerated by V_{Lab}, which is the dc bias between the source hexapole and collision cell octopole. The doubly-charged cations have a kinetic energy of $E_{Lab} = 2 \times V_{Lab}$, and the energy available for the reactions to occur is the kinetic energy in the center-of-mass (CM) frame, $E_{CM} = E_{Lab} \times m/(m + M)$, where m is the mass of the neutral Xe collision gas and M is the mass of the ionic reactant. The absolute zero of energy was measured in each individual experiment using a retarding potential on the octopole.(Ervin & Armentrout, 1985) The kinetic energy distribution of the ion beam was obtained by taking the derivative of the normalized ion intensity versus kinetic energy and fitting to a Gaussian distribution (generally less than 0.2 eV in full width at half maximum).(Ervin & Armentrout, 1985) All energies below are reported in the CM frame unless otherwise stated.

C. Thermochemical analysis. To extract thermochemical information from the kinetic energy dependent cross sections, there are several factors that were accounted for: multiple precursor ion-neutral collisions, lifetime effects, and any additional energy distributions. To ensure that the cross sections correspond to single ion-molecule collision events, the TCID reaction cross sections were linearly extrapolated to zero pressure from data sets acquired at various low pressures of Xe.(Hales, et al., 1990;Schultz & Armentrout, 1991) The total zero-pressure extrapolated reaction cross sections were modeled using the empirical threshold model shown in Eq. (3):

$$\sigma_j(E) = \sigma_{0,j} \sum g_i \left(E + E_i - E_{0,j}\right)^n / E \quad (3)$$

where $\sigma_{0,j}$ is an energy-independent scaling factor for product channel j, E is the relative translational energy of the reactants (E_{CM}), $E_{0,j}$ is the reaction threshold for channel j at 0 K, and n is an adjustable fitting parameter that describes the efficiency of the energy transfer upon collision.(Muntean & Armentrout, 2001) The summation is over the ro-vibrational states of the

$M^{2+}(H_2O)_x$ reactant with excitation energies E_i and populations g_i, where $\Sigma g_i = 1$. Ro-vibrational states were directly counted using the Beyer-Swinehart-Stein-Rabinovich algorithm to evaluate the internal energy distribution of the reactants.(Beyer & Swinehart, 1973;Stein & Rabinovich, 1977;Stein & Rabinovitch, 1973) A Maxwell-Boltzmann distribution at 300 K was used to compute the relative populations, g_i. Regarding lifetime effects, as the ions become larger and more complex, those with energy in excess of the dissociation energy $E_{0,j}$ may not have enough time to dissociate on the time scale of the experiment, $\tau \approx 5 \times 10^{-4}$ s. This effect results in a kinetic shift or delayed onset in the apparent threshold for CID. To account for this effect, Rice−Ramsperger−Kassel−Marcus (RRKM) statistical theory(Gilbert & Smith, 1990;Holbrook, et al., 1996;Truhlar, et al., 1996) for unimolecular dissociation was incorporated into the empirical threshold model, as shown in Eq. (4).(Rodgers, et al., 1997)

$$\sigma_j(E) = \left(\frac{n\sigma_{0,j}}{E}\right) \sum g_i \int_{E_{0,j}-E_i}^{E} \left[\frac{k_j(E^*)}{k_{tot}(E^*)}\right] (E-\varepsilon)^{n-1}\ P_{D1} d(\varepsilon) \quad (4)$$

In Eq. (4), ε is the energy transferred into internal degrees of freedom of the reactant ion during collision, such that the energized molecule (EM) has an internal energy of $E^* = \varepsilon + E_i$. $k_{tot}(E^*)$ is the total unimolecular dissociation rate constant, which was used to calculate the dissociation probability, $P_{D1} = 1 - \exp[-k_{tot}(E^*)\tau]$, and is defined in Eq. (5).

$$k_{tot}(E^*) = \sum_j k_j(E^*) = \sum_j s_j N_j^{\dagger}(E^* - E_{0,j})/h\rho(E^*) \quad (5)$$

Here, $k_j(E^*)$ is the rate constant for a single dissociation channel j, s_j is the reaction degeneracy calculated from the ratio of rotational symmetry numbers of the reactants and products of channel j,(Gilbert & Smith, 1990) $N_j^{\dagger}(E^* - E_{0,j})$ is the sum of ro-vibrational states of the transition state (TS) at an energy ($E^* - E_{0,j}$) above the threshold for channel j, h is Planck's constant, and $\rho(E^*)$ is the density of states of the EM at the available energy, E^*.(Gilbert & Smith, 1990) When the rate of dissociation is much faster than the average experimental time scale, Eq. (4) reduces to Eq. (3). Eq. (4) also naturally accounts for the competition between multiple dissociation pathways, e.g., reactions (1) and (2), using the $k_j(E^*)/k_{tot}(E^*)$ ratio.(Rodgers & Armentrout, 1998;Rodgers, et al., 1997)

In order to calculate the RRKM unimolecular rate constants in Eq. (5), ro-vibrational states of the EM and TS are required. Quantum chemical calculations were utilized to get the molecular parameters of the reactant ion for the EM. For the loss of water in reaction (1), a loose TS was used because there is no reverse activation barrier, a consequence of the heterolytic bond cleavage with the charge remaining on the metal containing fragment.(Armentrout & Simons, 1992) Thus, the water loss TS was treated in the phase space limit (PSL)(Rodgers, et al., 1997) because it is product-like and hence used molecular parameters taken from quantum chemical calculations of the products. Unlike the loose TS involved in the water loss process, the charge separation process (2) must pass over a Coulomb barrier to dissociate into two singly-charged species, i.e., there is a tight TS. The rate-limiting TSs for charge separation are labeled according to the products formed in reaction (2), i.e., TS[y + (x – y – 1)] where y is the number of water molecules attached to the MOH^+ product and (x – y – 1) is the number of water molecules attached to the H^+ product. Molecular parameters for these tight TSs were taken directly from calculations.

In addition to analyzing the total TCID cross sections for loss of the first water ligand, a sequential dissociation model(Armentrout, 2007) was employed to simultaneously analyze cross sections for the first and second water losses for a given complex size. The sequential model utilizes a statistical approach that has been shown to provide reasonably accurate thresholds for ligand loss from both singly and doubly charged systems.{Dalleska, 1994 #219;Hofstetter, 2013 #2316;Coates, 2017 #3325;Sweeney, 2015 #3074;Cooper, 2009 #3764;Cooper, 2011 #2210;Sweeney, 2014 #3041;Rodgers, 1997 #1;Armentrout, 2007 #1437} In this analysis, the BDE for the $M^{2+}(H_2O)_{x-1}$ complex is the difference between the threshold energies of these two product cross sections. The sequential threshold model combines Eq. (4), the cross section of the primary dissociation product, with the probability for further dissociation given by Eq. (6),

$$P_{D2} = 1 - e^{-k_2(E_2^*)\tau} \quad (6)$$

where $k_2(E_2^*)$ is the rate constant for sequential dissociation of a primary product ion having an internal energy of E_2^*. This energy was determined by energy conservation $E_2^* = E^* - E_{0,j} - T_1 - E_L$, where T_1 is the translational energy of the primary products and E_L is the internal energy of the

primary neutral product (here, H_2O). As discussed elsewhere, the distributions in these energies are assigned on the basis of statistical considerations.(Armentrout, 2007) Representation of this sequential dissociation model that combines Eqs. (4) and (6) will be notated as Eq. (4 × 6). In this review, the smallest cluster size of each metal dication was analyzed using sequential modeling in competition with the CS reaction. For some metal dications, smaller complexes cannot be generated in our ESI source because complexes at the critical size dissociate preferentially by CS yielding only singly-charged species.

The CID cross section models of Eqs. (4) and (4 × 6) were convolved with the relative kinetic energy distributions of the $M^{2+}(H_2O)_x$ and Xe reactants for comparison with the experimental cross sections.(Ervin & Armentrout, 1985) A nonlinear least-squares fitting procedure was used to optimize the fitting parameters in each model. The uncertainties associated with the fitting parameters, $\sigma_{0,j}$, n, and $E_{0,j}$, were determined from modeling multiple data sets (at least eight zero pressure extrapolated cross sections for each system) and additional modeling of the cross sections by scaling the vibrational frequencies of the EM and TSs by ±10%, varying the best fit n value by ±0.1, scaling the experimental time-of-flight up and down by a factor of 2, and including the absolute uncertainty of the energy scale, ±0.05 eV (Lab). Because all sources of energy are accounted for in these analyses, the measured thresholds, $E_{0,j}$, equal the BDE at 0 K for the $M^{2+}(H_2O)_x$ complex dissociating as in reaction (1) or the height of the CS Coulomb barrier of reaction (2).(Dalleska, Honma, et al., 1993)

D. Computational details. All studies included in this review utilized theoretical calculations performed using the Gaussian suite of programs.(Frisch, et al., 2005; Frisch, et al., 2009;Frisch, et al., 2016) For most M, possible geometries of reactants and products of $M^{2+}(H_2O)_x$ were calculated and optimized using the B3LYP/6-311+G(d,p) level to obtain vibrational frequencies and rotational constants.(Becke, 1993;Ditchfield, et al., 1971) A simulated annealing procedure coupled with intuition was utilized to ensure that all possible structures, especially those involving second shell ligands, were located. For larger ions, M = Sr, Ba, and Cd, a quasirelativistic Stuttgart-Dresden (SDD) small core effective core potential (ECP)(Kaupp, et al., 1991) was used

along with the def2-TZVP basis set(Weigend & Ahlrichs, 2005) on the metal and water ligands, and geometries were obtained using B3LYP.(Carl, et al., 2010;Wheeler, et al., 2018) In all cases, the vibrational frequencies were scaled by 0.989 before being applied in the data analysis process.(Foresman & Frisch, 1996) The scaled values were also used in all zero-point energy and thermal corrections. In all published work, single point calculations were performed at B3LYP and MP2(full)(Möller & Plesset, 1934) levels of theory with 6-311+G(2d,2p) or SDD/def2-TZVP basis sets. Other levels of theory were also applied in some publications as detailed when needed. Relative energies of different structures were obtained from the single point calculations including zero-point corrections to yield 0 K values and thermal corrections to yield 298 K values. Basis set superposition errors (BSSE) were calculated for dissociation of the lowest energy structures at each level of theory in the full counterpoise (cp) limit.(Boys & Bernardi, 1970;van Duijneveldt, et al., 1994) In this review, GSs are generally determined by relative energies obtained using MP2(full) single point calculations because infrared multiple photon dissociation (IRMPD) studies of $Zn^{2+}(H_2O)_x$ complexes demonstrate that these provide accurate identification of the structures observed, whereas density functional theory (DFT) calculations do not in all cases.(Cooper, et al., 2010) In addition, reaction coordinate pathways were investigated to determine the Coulomb barrier heights for CS reactions at B3LYP and MP2(full) levels using the 6-311+G(2d,2p) basis set with geometries calculated at the B3LYP/6-311+G(d,p) level.

In this review, (*m*, *n*) is used to describe different isomers of $M^{2+}(H_2O)_x$ complexes, where *m* represents the number of water molecules in the first solvent shell and *n* represents the second solvent shell of each structure. When needed to distinguish isomers having second shell ligands further, an A/D nomenclature is used to describe the hydrogen bonding of water molecules in the complex. The water molecule can be a single (A) or double (AA) hydrogen bond acceptor and/or a single (D) or double (DD) hydrogen bonding donor with shells separated by an underscore (_).

III. RESULTS

A. Comparison of alkaline earth metal dication hydration enthalpies. Figure 1 compares the sequential hydration energies of the four alkaline earth metal dications (Mg^{2+}, Ca^{2+}, Sr^{2+}, and Ba^{2+}) with one to ten water molecules obtained from TCID experiments.(Carl & Armentrout, 2012;Carl & Armentrout, 2013;Carl, et al., 2010;Carl, et al., 2007;Wheeler, et al., 2018;Wheeler, et al., 2015) These hydration energies are tabulated in Table 1. For each metal, the hydration energies generally decrease with increasing ligation, a result of less charge on the metal resulting from electron donation from each water ligand. For almost all *x* studied for Group 2 metal dications, the hydration energies decrease as one moves down the periodic table ($Mg^{2+} > Ca^{2+} > Sr^{2+} > Ba^{2+}$). This correlates directly with an increasing ionic radius.(Shannon, 1976) Both of these effects demonstrate that the metal ligand interactions are mainly electrostatic.

Further examination of Figure 1 shows that for the complexes of Mg^{2+}, there is a relatively large decrease from $x = 4$ to 5 and then another from $x = 6$ to 7. The first jump suggests that four water ligands fit well around the relatively small Mg^{2+} dication and that addition of a fifth water is somewhat hindered. The second jump indicates that six waters can complete the first solvent shell with the seventh water starting a second solvent shell. This conclusion is consistent with studies by Williams and co-workers that $Mg^{2+}(H_2O)_6$ exhibited evidence at high temperatures for both a (6,0) and a (4,2) structure.(Rodriguez-Cruz, et al., 1999) As discussed further below, the (6,0) structure is the GS according to theory. Similar trends in the Ca^{2+} and Sr^{2+} hydration energies show a relatively large decrease between $x = 6$ and 7, again suggesting that six water ligands may comprise a complete first solvent shell. In contrast, the decline in the hydration energies for Ba^{2+} is fairly smooth from $x = 1$ to 7, a nearly constant decrease of 19 ± 4 kJ/mol per ligand.

Ground structures (GSs) of the alkaline earth metal dication water complexes were investigated computationally, with results that generally match theoretical calculations previously published in all cases. The calculated M-O bond lengths between the metal dications and the water molecules are listed in Table 2 for the lowest energy isomers where the water ligands bind directly to the metal center, i.e., there are only inner shell ligands. For the smaller Mg^{2+} and Ca^{2+} ions, the maximum number of ligands in the inner shell is 6, whereas the maximum number found for the

larger Sr^{2+} is 7 and Ba^{2+} can accommodate 8 water ligands in the inner shell. The calculated bond lengths can be used to better visualize the relationship between hydration energy and metal ionic radius. Figure 2 shows hydration energies as a function of the predicted bond lengths for $x = 1 – 8$ complexes where the water ligands bind to the metal center directly. For $x = 1 – 4$, it can be seen that the hydration energies decrease uniformly as the metal-oxygen bond length increases and that the difference between the metals gets smaller as the number of ligands increases (slope becomes shallower). The linear trend observed for $x = 1 – 4$ is not maintained for all four metals at $x = 5$, which can be attributed to the steric hindrance among the ligands for the smallest metal dication, Mg^{2+}, consistent with the discussion above.

According to the quantum chemical calculations, all four alkaline earth metal dications with one water molecule have C_{2v} symmetry with the dipole of water directed at the metal cation. M-O bond lengths between the dication and the water ligand increase as the dication radii increase: 1.942, 2.244, 2.418, and 2.602 Å, respectively for Mg^{2+}, Ca^{2+}, Sr^{2+}, and Ba^{2+}. This increase directly parallels the increase in the ionic radius of M^{2+},(Shannon, 1976) Table 2, which is 1.24 ± 0.02 Å smaller for all four metals. No hydration energy of bare Mg^{2+} is available from any experiment. For TCID studies, this is because neither $Mg^{2+}(H_2O)$ nor $Mg^{2+}(H_2O)_2$ could be formed experimentally in our source, a result of $Mg^{2+}(H_2O)_3$ decomposing preferentially to $MgOH^+(H_2O)$ + H_3O^+, as discussed further below. Interestingly, the good correlation exhibited in Figure 2 suggests that an "experimental value for $D_0(Mg^{2+}\text{-}OH_2)$ can be derived by extrapolating the data on the $x = 1$ line. This yields an approximate value of 310 ± 30 kJ/mol, which is in reasonable agreement with the MP2(full)/6-311+G(2d,2p)//B3LYP/6-311+G(d,p) theoretical value of 319 kJ/mol.(Carl & Armentrout, 2013)

The $Mg^{2+}(H_2O)_2$ GS was predicted to have a linear geometry with D_{2d} symmetry, whereas the other three alkaline earth dication complexes prefer a bent geometry, with O-M-O bond angles near 120°: 125°, 117°, and 122° as one moves down the periodic table, Figure 3. This behavior is attributed to polarization of the core electrons on these alkaline earth dications, which enhances the effective charge on the metal and thereby compensates for the increased ligand-ligand

repulsion in the bent structure.(Bauschlicher, et al., 1992;Glendening & Feller, 1996;Klobukowski, 1992) In essence, the electron donation of the ligands leads to polarizing the metal core electrons away from the incoming ligands such that they occupy a ligand site, which pushes the ligands away from a linear arrangement. The same effect(Bauschlicher, et al., 1992) occurs for $M^{2+}(H_2O)_3$ complexes where the M = Mg and Ca structures have D_3 symmetry in which all heavy atoms are located in the same plane with bond lengths at 1.987 and 2.313 Å, respectively. In contrast, Sr^{2+} and Ba^{2+} with three water ligands adopt C_3 symmetry structures where the metal dications are located above the plane containing the oxygen atoms of the three water molecules (bond lengths are 2.487 and 2.680 Å), Figure 3. For all four metals, bond lengths are uniformly 1.30 ± 0.03 Å larger than the M^{2+} radii. In all of these structures, the water molecules are tilted to enable weak hydrogen bonding interactions between adjacent ligands.

Upon the addition of a fourth water ligand, $M^{2+}(H_2O)_4$, all alkaline earth metals examined favor a tetrahedral structure with respect to the oxygen atoms with pseudo S_4 symmetry. Bond lengths again track the ionic radii, exceeding them by 1.34 ± 0.03 Å. Again, water molecules in these structures are tilted to enable weak hydrogen bonding interactions between adjacent ligands. For x = 5, all alkaline earth metal dications have similar structures where water ligands have a square pyramidal orientation with respect to the oxygen atoms and overall C_{2v} symmetry. Starting at x = 5, the absolute hydration energies for Group 2 dications are closer to each other but still display a decrease as the ionic radii increase (difference of 1.38 ± 0.02 Å), Figure 2. Here, the hydrogen bonding effect is clearer as the four water ligands in the base alternate whether parallel to the base or perpendicular. The single apex water ligand then directs its hydrogens towards the two base ligands with which it can hydrogen bond.

For $M^{2+}(H_2O)_6$ (M = Mg, Ca, Sr, Ba), the structures are octahedral with respect to the oxygen atoms with M-O bond lengths of 2.113, 2.405, 2.582, and 2.784 Å, respectively, 1.41 ± 0.02 Å larger than the metal dication radii. The complexes all have near T_h symmetry including the hydrogen atoms because there are weak hydrogen bonding interactions with adjacent water molecules. For Mg^{2+} and Ca^{2+}, six is the maximum number of water ligands in the inner shell. For

the three smaller metal dications, the BDEs are similar to each other: 97 ± 8 kJ/mol for Mg^{2+}, 99 ± 9 kJ/mol for Ca^{2+}, and 94 ± 3 kJ/mol for Sr^{2+}, whereas it is 77 ± 6 kJ/mol for Ba^{2+}, 17 – 22 kJ/mol lower than other three alkaline earth metal dications. As for x = 5, the linear trend in hydration energies versus r(M-O) is disrupted for Mg, Figure 2, again presumably a consequence of steric crowding. Indeed, calculations now indicate that a (5,1) structure with one ligand in the second solvent shell is low in energy and can be the GS at 298 K (according to B3LYP single point energies by 6 kJ/mol) because this structure is entropically more favorable than the (6,0) octahedral structure. MP2 theory suggests the (5,1) structure lies only 5 kJ/mol above its (6,0) GS at 298 K.(Carl & Armentrout, 2013)

The larger Group 2 ions, Sr^{2+} and Ba^{2+}, can have seven water molecules directly bind to the metal center. Here, average M-O bond lengths are 2.617 Å for Sr^{2+} and 2.811 Å for Ba^{2+} as predicted by theoretical calculations, which again tracks the metal dication size (1.45 ± 0.02 Å smaller). The GS has C_2 symmetry, Figure 3. For Mg^{2+} and Ca^{2+}, the GSs of the seven water complexes are (6,1) geometries with one water ligand in the second solvent shell, Figure 3. Note that this structure partially disrupts the hydrogen bonding of the inner solvent shell. For both x = 7 and 8, the BDEs remain similar but continue to decrease as the ionic radii increase. For $M^{2+}(H_2O)_8$, Mg^{2+} and Ca^{2+} both have (6,2) geometries, $Sr^{2+}(H_2O)_8$ has a (7,1) geometry, and $Ba^{2+}(H_2O)_8$ was predicted to have an (8,0) geometry according to MP2 theory but (6,2) according to B3LYP. Eight is the largest number of water ligands in the inner solvent shell of the four alkaline earth metal dications. Note that the hydration energies nearly plateau for x = 7 – 9, which has been attributed to the likelihood that all three complex sizes have these ligands bind in the second solvent shell to two inner shell ligands for both Mg^{2+} and Ca^{2+}, which are calculated to have (6,3) geometries for x = 9. The larger Sr^{2+} ion has a (7,2) GS geometry. It can be seen that the BDE for $Mg^{2+}(H_2O)_{10}$ is smaller than those for x = 7 – 9, which is attributed to a (6,4) geometry in which two pairs of outer shell water ligands share hydrogen bonds with a pair of inner shell ligands: (6,4)_2DD,4D_4AA.

Hydration energies of alkaline earth metals have also been investigated experimentally by Kebarle and co-workers using high pressure mass spectrometry (HPMS)(Peschke, et al., 1998) and by Williams and co-workers using Blackbody Infrared Radiative Dissociation (BIRD),(Rodriguez-Cruz, et al., 1999) Table 1. Because these techniques rely on thermal equilibria, values for many inner shell ligands are inaccessible. The hydration values for $M^{2+}(H_2O)_x$ (M = Mg, Ca, Sr, Ba) where $x = 4 - 10$ are compared to those from TCID experiments in Table 1. Overall, the values obtained from the three methods are generally within combined uncertainties of each other. Mean absolute deviations (MADs) between TCID and HPMS are 7.4 kJ/mol (while combined experimental uncertainties are 7.9 kJ/mol), whereas the deviations of BIRD values from TCID are 6.3 kJ/mol (compared to 8.3 kJ/mol for the combined experimental uncertainties). For the smaller complexes ($x \leq 6$), better agreement is generally found with MADs of 4.0 kJ/mol for both HPMS and BIRD. For the larger complexes ($x > 6$), the TCID values are systematically below both HPMS and BIRD results by averages of 9.0 and 8.3 kJ/mol, respectively, just outside the combined experimental uncertainties. In most cases, these complexes involve outer shell ligands, potentially making them more problematic to study. It is possible that this difference is because the TCID complexes are not fully thermalized in our ESI source; but because the BIRD and HPJMS values are done over a range of temperatures, it is also possible that the higher temperatures used begin to form complexes that are entropically favored. The effects of multiple structures were not always considered in the interpretation of these studies, although BIRD studies of $Mg^{2+}(H_2O)_6$ complexes did identify multiple isomers.(Rodriguez-Cruz, et al., 1999)

B. Comparison of late 3d transition metal dication hydration enthalpies. Figure 4 compares the TCID experimental 0 K BDEs for $M^{2+}(H_2O)_x$ complexes of $Mn^{2+}(3d^5)$,(Yang, et al.) Fe^{2+} $(3d^6)$,(Hofstetter & Armentrout, 2013) $Co^{2+}(3d^7)$,(Coates & Armentrout, 2018) $Ni^{2+}(3d^8)$,(Coates & Armentrout, 2017) $Cu^{2+}(3d^9)$,(Sweeney & Armentrout, 2014;Sweeney & Armentrout, 2015) and $Zn^{2+}(3d^{10})$,(Cooper & Armentrout, 2009;Cooper, et al., 2009) to highlight the periodic trends. These values are listed in Table 3. Clearly, as for the alkaline earths (included in Figure 4 as the line showing values for Mg^{2+}), the general trend is that hydration energies

decrease as the complex size increases (the single exception is for Co^{2+} from $x = 5$ to 6, which will be discussed below). This trend can be explained as the bonds weaken with addition of each water ligand because the added electron density decreases the effective charge on the metal dication. This systematically increases the bond length between the metal dication and the oxygen, as listed in Table 4 from B3LYP/6-311+G(d,p) calculations. In all cases, these calculations correspond to high-spin states as water is a weak-field ligand (as verified by the calculations in all systems).

For all of these metals, complexes of smaller size than listed in Table 3 could not be acquired experimentally because, at the critical size (discussed below), these complexes dissociated by the charge separation reaction (2) rather than by loss of water ligands. It can also be noted that the only alternative experimental values for all these complexes available in the literature are those for Ni^{2+}, as obtained using HPMS and BIRD. HPMS values are 73 ± 4 kJ/mol for $x = 8 – 10$ and 68 ± 4 kJ/mol for $x = 11$,(Blades, et al., 1990;Blades, et al., 1990) BIRD values for $x = 6 – 8$ are 101 ± 4, 74 ± 3, and 72 ± 3 kJ/mol, respectively.(Rodriguez-Cruz, et al., 1998) All three approaches yield very similar hydration energies for $x = 8$ and the BIRD values are within the combined experimental uncertainties of the TCID values. The HPMS values for $x = 9 – 11$ lie well above the TCID values. Theory agrees better with the HPMS value for $x = 9$ and with the TCID value for $x = 11$.(Coates & Armentrout, 2017)

Figure 4 illustrates that the hydration energies for larger complexes ($x \geq 7$) are essentially equivalent for all metals, within experimental uncertainty of each other (with exceptions at Cu($x = 7$) and perhaps Mn($x = 9$). This trend is not unexpected as all these transition metals have similar dication radii (Table 4) and these ligands are predicted be in the second solvent shell. Thus, the BDEs for all these metals at large x values are primarily determined by losses of water ligands that are accepting hydrogen bonds from one or two inner shell waters.

The exception of Cu($x = 7$) probably relates to a different structure. The structure of $M^{2+}(H_2O)_7$ for most metals is the (6,1) structure shown in Figure 3 for Mg. MP2 theory predicts this is the GS for complexes of Mn, Fe, Co, and Ni. (In some cases, other levels of theory make other predictions but MP2 theory provided the most accurate predictions for $Zn^{2+}(H_2O)_x$ structures

in an IRMPD study.(Cooper, et al., 2010)) Zn prefers a five-coordinate (5,2)_4D_2AA structure with the two second shell waters making hydrogen bonds with two pairs of inner shell water ligands. In contrast, because Cu^{2+} has a $3d^9$ configuration with the highest crystal field stabilization energy as determined in the Irving-Williams series,(Irving & Williams, 1953) the partially filled e_g orbitals in the $3d^9$ configuration tend to destabilize the axial ligands in an octahedral ligand environment. Thus, Cu^{2+} prefers to have square-planar inner shell coordination. Indeed, calculations predict that $Cu^{2+}(H_2O)_7$ has a (4,3)_2DD,2D_3AA structure in which there are four inner shell water ligands in a square planar geometry around the central metal dication and the three second shell waters make two hydrogen bonds with pairs of inner shell ligands, as presented in Figure 5. This structure was confirmed by IRMPD results.(O'Brien & Williams, 2008) Because there are only four inner shell water ligands (compared to 6 for most other metals and 5 for Zn), the polarization of the inner shell ligands and hence the binding of the outer shell water is potentially enhanced in this case. One might expect the same to be true for x = 8, where the structure is (4,4)_4DD_4AA with D_{4h} symmetry, Figure 5. Indeed, theory predicts that the 7th and 8th water ligands have very similar binding energies (differing by 5.5 ± 1.7 kJ/mol for four levels of theory) whereas the experimental difference is 28 ± 5 kJ/mol. This suggests that the experimental value for x = 7 may be slightly high and that for x = 8 is somewhat low. Note that for Cu, the hydration energies for x = 9 and 10 are similar to one another and drop 23 kJ/mol from x = 8, consistent with needing to place these ligands in a third solvent shell or in the weakly bonding axial position.

In contrast to the similarity in hydration energies for the larger complexes, the smaller ones (x = 4 – 6) show much larger differences. For x = 6, the BDEs increase steadily from Mn^{2+} to Fe^{2+} to Co^{2+} to Ni^{2+} and then drop for Zn^{2+}. These changes can be assigned to the expected trend for (6,0) complexes as the metal dication gets smaller (because of the increasing nuclear charge as one moves across the periodic table), 0.83 to 0.78 to 0.74 to 0.69 and then back up to 0.74 Å, respectively.(Shannon, 1976) Here, Zn may differ slightly because IRMPD studies indicate that the (6,0) and (5,1) structures are both probably populated.(Cooper, et al., 2010)

In contrast, for $x = 5$, the BDE for Co^{2+} is slightly lower than those for Mn^{2+} and Fe^{2+}, which are lower than that of Ni^{2+}. The very different trend for $x = 5$ can be attributed to the differing coordination numbers of the different metals, as manganese, iron, and nickel have all five water ligands directly bound to the metal ion in (5,0) structures and roughly follow the same increasing BDE trend exhibited for $x = 6$. In contrast, for cobalt, the fifth water is more weakly bound in the second solvent shell in a (4,1) structure. At $x = 4$, all geometries are predicted to be (4,0), but the BDEs do not follow the nuclear charge trend seen for $x = 6$ because the geometries are actually distinct. For Mn^{2+} ($3d^5$), Fe^{2+} ($3d^6$), and Co^{2+} ($3d^7$), the (4,0) complexes have near-tetrahedral symmetry with respect to the oxygens, although the different 3d orbital populations induce some distortions, i.e., ∠OMnO = 107° and 111°, ∠OFeO = 108° and 110°, and ∠OCoO = 105° and 112°. Thus, the hydration energies of these three complexes are similar and the distortions mean the nuclear charge trend is not followed. In contrast, calculations for Ni^{2+} ($3d^8$) showed that the triplet state (4,0) complex has a see-saw geometry with singly occupied molecular orbitals (SOMOs) in octahedral-like e_g MOs. The distortion and increased ligand–ligand repulsion for Ni^{2+} explain the smaller BDE at $x = 4$.

C. Comparison of Zn and Cd metal dication hydration enthalpies. Cadmium is known to deactivate proteins and enzymes (where it displaces another group 12 element, Zn), bioaccumulate, and its anthropogenic emissions have been estimated to be 18 times higher than naturally occurring rates.(Fergusson, 1990;Salomons, et al., 1995) Therefore, it has been classified as a priority pollutant by the U.S. environmental protection agency. TCID studies of $Cd^{2+}(H_2O)_x$ complexes include $x = 3 - 11$.(Cooper & Armentrout, 2011;Cooper & Armentrout, 2010) The resultant 0 K hydration energies for Cd^{2+} ($4d^{10}$) are listed in Table 3 and compared to those for Zn^{2+} ($3d^{10}$) (and Mg^{2+}) in Figure 6. Not surprisingly, the overall trend in hydration energies matches those discussed above. As for the other metal ions, the hydration energies of all the metals are similar for $x \geqslant 7$. For $x = 6$, the smallest complex available for Zn, the Cd hydration energy is slightly (8 kJ/mol) lower, but this is reasonable considering that the ionic radii are not drastically different, with Cd^{2+} (0.95 Å) being slightly larger than Zn^{2+} (0.74 Å).(Shannon, 1976) Therefore,

one anticipates that the inner shell hydration energies of Zn^{2+} will lie above those found for Cd^{2+}. Indeed, for these smaller complexes ($x < 6$), the Cd hydration energies fall below those for Mg^{2+}, Figure 6, as expected from the ionic radii. Thus, biological systems should be sensitive to substitution of Zn^{2+} by Cd^{2+} only when the number of ligands surrounding the metal is relatively small.

D. Critical sizes for $M^{2+}(H_2O)_x$. As mentioned above, at a particular complex size, in addition to losing a single water ligand, $M^{2+}(H_2O)_x$ can dissociate into two singly-charged species in reaction (2). This type of reaction has also been investigated by Kebarle and coworkers(Blades, et al., 1990;Blades, et al., 1990;Jayaweera, et al., 1990;Peschke, et al., 1999) and Shvartsburg and Siu,(Shvartsburg & Siu, 2001) although none of these studies is able to directly link the reactants or products of reaction (2). The x_{crit} for hydrated Group 2 and transition metal dications from both groups are compared with those extracted from GIBMS studies in Table 5. As first postulated by Kebarle and co-workers,(Blades, et al., 1990;Blades, et al., 1990), there is a rough correlation of x_{crit} with the second ionization energy (2IE) of the corresponding metal.

Of these metals, barium is the only one where no CS reaction was observed by Kebarle and co-workers, hence $x_{crit} = 0$. Kebarle and co-workers attributed this to the low 2IE of Ba, such that $Ba^{2+}(H_2O)_2$ can only fragment by water loss to yield $Ba^{2+}(H_2O)$. In contrast, Shvartsburg and Siu observed that the dominant dissociation process for $Ba^{2+}(H_2O)_x$ was water loss reactions but they also observed the formation of $BaOH^+$.(Shvartsburg & Siu, 2001) They attributed this singly-charged species to be a product of $Ba^{2+}(H_2O)_2$, therefore x_{crit} for Ba^{2+} was assigned as 2. This dichotomy was resolved by the TCID studies where specific $Ba^{2+}(H_2O)_x$ complexes were individually isolated and dissociated in turn.(Wheeler, et al., 2015) Under ordinary source conditions, no $BaOH^+$ was observed for any complex size, consistent with the work of Kebarle and co-workers; however, under conditions where the in-source fragmentation process was set to maximize production of $Ba^{2+}(H_2O)_3$, reaction (7), formation of the $y+(x-y-1) = 0+2$ products, was observed with very low intensity, see Figure 7, consistent with the experimental observations of Shvartsburg and Siu but not with their assignment of x_{crit}.

$$Ba^{2+}(H_2O)_3 \rightarrow BaOH^+ + H^+(H_2O)_2 \quad (7)$$

In this particular case, the $H^+(H_2O)_2$ product was not observed in the TCID study because of the low intensity of the product channel coupled with unfavorable product collection conditions. (In the CS reaction, the large Coulomb barrier in the exit channel, corresponding here to TS[0+2], means that the ionic products should be formed with considerable kinetic energy release. Because of conservation of linear momentum, the light $H^+(H_2O)_2$ product has a much larger velocity than the heavy $BaOH^+$ product, which makes efficient data collection of the lighter product ion particularly challenging.) Modeling of the cross sections shown in Figure 7 suggested that reactions (1) and (2) compete but that reaction (2) should only be observed if TS[0+2] is slightly below (~0.1 eV) the threshold for reaction (1). As in the CS channels for all metals, the magnitude of the CS cross section is small because the tight TS[0+2] makes it entropically much less favorable than decomposition over the loose PSL TS for water loss. Notably, these source conditions also lead to a tail in the $Ba^{2+}(H_2O)_2$ product cross section, Figure 7, which is probably associated with an excited isomer, possibly the (2,1) or (1,1,1) complexes in which there are water ligands in outer shells.

As for many of the CS reactions studied, the potential energy surface for this process was investigated theoretically. The results from B3LYP/def2-TZVPP calculations are shown in Figure 8. Here, it can be seen that the rearrangement leading to reaction (7) requires moving water ligands to the outer shell, via the intermediates (2,1), (1,2), and finally (1,1,1) before passing over the TS[0+2] Coulomb barrier, which lies 1 kJ/mol below the water loss channel at this level of theory. Further, all levels of theory agreed that decomposition over TS[1+1] leading to $BaOH^+(H_2O)$ + H_3O^+ is much higher in energy than TS[0+2] and further that $Ba^{2+}(H_2O)_2$ should dissociate by water loss and not undergo CS.(Wheeler, et al., 2015) Thus, x_{crit} is determined to be 3 for Ba^{2+} given the energetic definition for the critical size.

In the Sr^{2+} system, the only complex observed to undergo CS was $Sr^{2+}(H_2O)_2$, which dissociates to $SrOH^+$ + H_3O^+, both of which are observed in equal amounts and have similar thresholds.(Carl, Chatterjee, et al., 2010) Although the apparent thresholds of the singly-charged

product cross sections lie above the apparent threshold for the water loss cross section, the charge separation products are probably energetically favored otherwise they would not be observed. Thus, the critical size for Sr^{2+} was assigned as 2, in agreement with previous conclusions, Table 5. Theory found that reaction (2) either had a comparable energy to that of reaction (1) (MP2) or slightly below (B3LYP).(Carl, Chatterjee, et al., 2010)

For the complexes of Ca^{2+}, $Ca^{2+}(H_2O)_2$ dissociated via both reactions (1) and (2), where the latter generated $CaOH^+ + H_3O^+$, again in equal amounts with the same thresholds.(Carl & Armentrout, 2012) The latter process had the lower threshold (by 57 ± 11 kJ/mol according to modeling of the experiment) in agreement with theory. This would be consistent with the assignments of $x_{crit} = 2$ made by both Kebarle and co-workers and Shvartzburg and Siu, Table 5. However, $Ca^{2+}(H_2O)_3$ was observed to dissociate predominantly by reaction (1) but also by reaction (8).

$$M^{2+}(H_2O)_3 \rightarrow MOH^+(H_2O) + H_3O^+ \quad (8)$$

Analysis of these cross sections yielded a threshold energy for reaction (8) lying 5 ± 12 kJ/mol lower than that for water loss, such that $x_{crit} = 3$. This relative energy agreed with B3LYP and B3P86 calculations, whereas MP2 predicted the opposite result by 17 kJ/mol.(Carl & Armentrout, 2012)

Mg has the largest 2IE among the Group 2 metals. $Mg^{2+}(H_2O)_3$ dissociated primarily via reaction (8), with thresholds for both products lying well below that for reaction (1). $Mg^{2+}(H_2O)_4$ was also observed to dissociate to $MgOH^+(H_2O)_2 + H_3O^+$, but this process is much less efficient than reaction (1) and has a higher apparent threshold. However, competitive analysis of these cross sections indicated that the CS reaction had a threshold energy lying 4 ± 6 kJ/mol *below* that for reaction (1). Thus, the x_{crit} of Mg^{2+} is 4.

The Group 2 metals have the lowest 2IEs among the metal dications studied. Transition metals have higher 2IEs that increase from Mn to Cu with that for Zn lying between Co and Ni, Table 5. Cu has the largest 2IE because the second electron is removed from a full $3d^{10}$ shell. In the $Mn^{2+}(H_2O)_x$ systems, $x = 3 – 5$ are observed to dissociate by both reaction (1) and reaction (2),

where the products are 1+1, 2+1, and 2+2, respectively.(Yang, et al.) Analysis of the cross sections found that the CS processes were thermodynamically favored for x = 3 and 4, but not for x = 5. Thus, Mn has a critical size of 4 corresponding to reaction (9).

$$M^{2+}(H_2O)_4 \rightarrow MOH^+(H_2O)_2 + H_3O^+ \quad (9)$$

$Cd^{2+}(H_2O)_x$ systems exhibit the same three CS reactions and likewise behave very similarly, with the CS channel TS[2+2] for x = 5 measured to be only 3 ± 3 kJ/mol higher than loss of a water ligand.

Similarly, $Fe^{2+}(H_2O)_4$ undergoes reaction (2) to form the 2+1 products of reaction (9), but larger complexes of x = 5 – 8 also exhibit minor CS channels to yield 2+2, 3+2, 3+3, and 4+3 products, respectively.(Hofstetter & Armentrout, 2013) In this system, a competitive analysis of the cross sections for reactions (1) and (2) was not possible because of experimental complications (e.g., $Fe^{2+}(H_2O)_5$ and $H^+(H_2O)_4$ are isobaric and both are produced in the ESI source). A quantitative comparison of the experimental results with theoretical predictions suggested that MP2 theory predicted the relative energies for these two competing channels better than density functional approaches. This led to the conclusion that x_{crit} = 4 for Fe although decomposition of x = 5 by CS is only slightly (1 kJ/mol) disfavored compared to loss of water according to MP2 theory.

In the Co^{2+} complexes, the x = 7 complex dissociated primarily by reaction (1) but also formed the 3+3 CS products, and the x = 6 complex dissociated by reaction (1) but formation of the 3+2 products in reaction (10) was appreciable.(Coates & Armentrout, 2018)

$$Co^{2+}(H_2O)_6 \rightarrow CoOH^+(H_2O)_3 + H(H_2O)_2^+ \quad (10)$$

There was also evidence for reaction (9) at higher energies. Competitive analysis of the x = 6 and 7 complexes found that the 3+2 CS products of x = 6 had a lower threshold than reaction (1) whereas for x = 7, the processes were nearly isoenergetic, with the 3+3 TS lying 2 ± 3 kJ/mol above the water loss channel. Thus, Co has x_{crit} = 6. This value is higher than the those found by Kebarle and coworkers, x_{crit} = 4, and Shvartzburg and Siu, x_{crit} = 5, but these assignments are largely predicated on $CoOH^+(H_2O)_3$ being the largest complex observed and the assumption that H_3O^+ is the accompanying product. A similar comparison occurs for Zn^{2+}, where x_{crit} = 7 is

assigned from TCID studies,(Cooper, et al., 2009) whereas previous results suggested 5 or 6, Table 5. Here, $Zn^{2+}(H_2O)_7$ dissociates by both reaction (1) and the 3+3 CS process shown in reaction (11).

$$M^{2+}(H_2O)_7 \rightarrow MOH^{+}(H_2O)_3 + H(H_2O)_3^{+} \quad (11)$$

The CS process is clearly favored enthalpically (although still has a smaller cross section than water loss because of the entropic inhibition), by 11 ± 2 kJ/mol according to competitive modeling of the cross sections. The $x = 8$ complex also undergoes CS dissociation to form the 4+3 products, but now modeling indicates that the CS channel lies 5 ± 2 kJ/mol above the water loss channel.

Cu has the highest 2IE value of any metal examined in these studies, 20.3 eV. Here, the $x = 8$ complex dissociated by reaction (1) primarily but also the CS 4+3 reaction (12).(Sweeney & Armentrout, 2015)

$$Cu^{2+}(H_2O)_8 \rightarrow CuOH^{+}(H_2O)_4 + H(H_2O)_3^{+} \quad (12)$$

Competitive analysis of the cross sections indicates that the 4+3 CS process is favored over water loss by only 1 ± 2 kJ/mol, but uniformly needs to be lower to reproduce the intensity observed. A CS 3+3 reaction was also observed, potentially reaction (11); however, analysis suggested that these products resulted from subsequent decomposition of the $CuOH^{+}(H_2O)_4$ product of reaction (12).

Overall, the critical size of the metals studied vary roughly in accord with the second IEs, as illustrated in Table 5. The only notable exception is Ni, where $x_{crit} = 4$, like that of Mn and Fe, but below those of the metals adjacent in 2IE, Zn ($x_{crit} = 7$) and Cu ($x_{crit} = 8$). $Ni^{2+}(H_2O)$ complexes were observed to undergo CS reactions for $x = 4$ (2+1), 5 (2+2), and 6 (3+2). This study was complicated by the generation of excited isomers of many of the complexes, typically those having one water molecule in the second solvent shell, (x-1,1) structures. CS reactions were only observed when the lower energy (x,0) structures were dominant. Competitive analysis of the cross sections indicated that for $x = 5$ and 6, the CS channels have higher thresholds than reactions (1), and the experimental observations for $x = 4$ indicated that the CS threshold was lower, hence $x_{crit} = 4$. We conclude that either the rough correlation with 2IE observed is not rigorous (and indeed, the origins

of the correlation have not been detailed) or that the preference for square planar coordination of $Ni^{2+}(3d^8)$ permits more facile rearrangement of water ligands into the second shell, as needed for the CS reaction to occur.

As shown in Table 5, critical values obtained from the TCID experiments are often larger than the values obtained by other groups. As discussed above, previous observations were often tied to observation of only the largest $MOH^+(H_2O)_y$ species in their mass spectrum, with no means to ascertain the accompanying $H^+(H_2O)$ product or the precursor. The GIBMS experiments clearly identify the precursor for each CS channel and the kinetic energy dependence allows the two products to be uniquely paired.

As Table 5 shows, for the transition metal dications, the critical sizes can reach large numbers, which means that dissociation of these complexes in the ion source will form the energetically-favored singly-charged metal hydroxide ions rather than losing water ligands to yield smaller $M^{2+}(H_2O)_x$ complexes. Therefore, as listed in Table 3, our TCID experiments have not been able to measure the hydration energies of the smaller complexes of these metals. Alternative ion production methods might be able to overcome this limitation.

IV. CONCLUSION

This review provides an in-depth look at the hydrated metal dications that have been studied by the Armentrout group using TCID in a GIBMS. The Group 2 alkaline earth metals have hydration energies that decrease as the ion radius increases and that decrease as the number of ligands increases, until clusters of $x \geqslant 7$ which have similar hydration energies. The same general trend exists for late first-row 3d transition metals with few exceptions, notably the (4,1) GS for $Co^{2+}(H_2O)_5$ differs from the (5,0) structure of the others, leading to a weaker BDE. The other notable trend observed was for $x = 6$. The hydration energies of the transition metals for this cluster size increase from Mn^{2+} to Ni^{2+} as they have the same GSs (octahedral geometries predicted by theoretical calculations) but have decreasing metal ionic radii. A decrease is then observed for Zn^{2+} because its ionic radius increases again, a consequence of the $3d^{10}$ filled shell electronic

configuration. For clusters of $x \geq 7$, the hydration energies are similar to each other and similar to those for the alkaline earths. Although remnants of the periodic trends observed for smaller complexes (involving only first shell ligands) remain, these variations are small, suggesting that studies of additional metal dications should not differ widely from the values documented here for these larger complex sizes.

The critical sizes of these eleven metal dication-water complexes are compared with previously published reports from Kebarle and co-workers and Shvartsburg and Siu in Table 5. The main advantage of the TCID studies compared with previous work is the ability to link the singly-charged products with each other (via their energy dependent cross sections) and with the corresponding reactants. Previous reports generally relied on the observation of the largest $MOH^+(H_2O)_y$ complex in their assignment of x_{crit} (implicitly assuming H_3O^+ was the accompanying product). The TCID studies also allow an evaluation of the relative energetics of the charge separation reactions (2) and those for water loss in reaction (1), which then permits a more precise energetic definition of the critical size. Further, the detailed reaction pathways for the various charge separation processes observed were investigated theoretically for each metal-dication reactant. Combining these potential energy surfaces and modeling of the experimental data provides a clear understanding of the competition between charge separation and water loss processes. This procedure also resolves the discrepancies in assignment of critical sizes of the metal dication complexes as previously analyzed. As shown for example in Figure 8, these pathways can be quite complex (thereby making them entropically disfavored, in agreement with observation), but agreement between theory and experimental energies for the CS transition states provides good evidence that the pathways elucidated match experimentally observed processes.

V. ACKNOWLEDGEMENT

Financial support for these studies has been provided by the National Science Foundation, most recently Grant No. 1954142. This work is in honor of Veronica Bierbaum, her many contributions to ion chemistry, and her friendship and counsel.

VI. REFERENCES

2006. NIST Atomic Spectra Database. NIST Atomic Spectra Database Levels Form. National Institute of Standards and Technology.

Anderson SG, Blades AT, Klassen J, Kebarle P. Determination of Ion-Ligand Bond Energies and Ion Fragmentation Energies of Electrospray-Produced Ions by Collision-Induced Dissociation Threshold Measurements. Int. J. Mass Spectrom. Ion Processes 1995; 141:217-228.

Aristov N, Armentrout PB. Collision-Induced Dissociation of Vanadium Monoxide Ion. J. Phys. Chem. 1986; 90:5135-5140.

Armentrout PB. Statistical modeling of sequential collision-induced dissociation. J. Chem. Phys. 2007; 126:234302.

Armentrout PB, Simons J. Understanding Heterolytic Bond Cleavage. J. Am. Chem. Soc. 1992; 114:8627-8633.

Bauschlicher CW, Sodupe M, Partridge H. A theoretical study of the positive and dipositive ions of $M(NH_3)_n$ and $M(H_2O)_n$ for M = Mg, Ca, or Sr. J. Chem. Phys. 1992; 96:4453-4463.

Becke AD. Density-functional Thermochemistry. III. The Role of Exact Exchange. J. Chem. Phys. 1993; 98:5648-5652.

Beyer TS, Swinehart DF. Number of Multiply-Restricted Partitions. Commun. ACM 1973; 16:379.

Blades AT, Jayaweera P, Ikonomou MG, Kebarle P. Ion-molecule Clusters Involving Doubly Charged Metal Ions (M^{2+}). Int. J. Mass Spectrom. 1990; 102:251-267.

Blades AT, Jayaweera P, Ikonomou MG, Kebarle P. Studies of Alkaline Earth and Transition Metal M^{++} Gas Phase Ion Chemistry. J. Chem. Phys. 1990; 92:5900-5906.

Boys SF, Bernardi R. The Calculation of Small Molecular Interactions by the Differences of Separate Total Energies. Some Procedures with Reduced Errors. Mol. Phys. 1970; 19:553-566.

Carl DR, Armentrout PB. Experimental Investigation of the Complete Inner Shell Hydration Energies of Ca^{2+}: Threshold Collision-induced Dissociation of $Ca^{2+}(H_2O)_x$ Complexes ($x = 2 – 8$). J. Phys. Chem. A 2012; 116:3802-3815.

Carl DR, Armentrout PB. Threshold Collision-Induced Dissociation of Hydrated Magnesium: Experimental and Theoretical Investigation of the Binding Energies for $Mg^{2+}(H_2O)_x$ complexes ($x = 2 – 10$). ChemPhysChem 2013; 14:681-697.

Carl DR, Chatterjee BK, Armentrout PB. Threshold Collision-induced Dissociation of $Sr^{2+}(H_2O)_x$ Complexes ($x = 1 – 6$): An Experimental and Theoretical Investigation of the Complete Inner Shell Hydration Energies of Sr^{2+}. J. Chem. Phys. 2010; 132:044303.

Carl DR, Cooper TE, Oomens J, Steill JD, Armentrout PB. Infrared Multiple Photon Dissociation Spectroscopy of Cationized Methionine: Effects of Alkali-Metal Cation Size on Gas-Phase Conformation. Phys. Chem. Chem. Phys. 2010; 12:3384-3398.

Carl DR, Moision RM, Armentrout PB. Binding Energies for the Inner Hydration Shells of Ca^{2+}: An Experimental and Theoretical Investigation of $Ca^{2+}(H_2O)_x$ Complexes ($x = 5 – 9$). Int. J. Mass Spectrom. 2007; 265:308-325.

Carl DR, Moision RM, Armentrout PB. In-source Fragmentation Technique for the Production of Thermalized Ions. J. Am. Soc. Mass Spectrom. 2009; 20:2312-2317.

Carpenter JE, McNary CP, Furin A, Sweeney AF, Armentrout PB. How Hot are Your Ions Really? A Threshold Collision-Induced Dissociation Study of Substituted Benzylpyridinium "Thermometer" Ions. J. Am. Soc. Mass Spectrom. 2017; 28:1876-1888.

Cheng ZL, Siu KWM, Guevremont R, Berman SS. Electrospray Mass Spectrometry: A Study on Some Aqueous Solutions of Metal Salts. J. Am. Soc. Mass Spectrom. 1992; 3:281-288.

Coates RA, Armentrout PB. Binding Energies of Hydrated Cobalt Hydroxide Ion Complexes: A Guided Ion Beam and Theoretical Investigation. J. Chem. Phys. 2017; 147:064305.
Coates RA, Armentrout PB. Binding Energies of Hydrated Cobalt(II) by Collision-Induced Dissociation and Theoretical Studies: Evidence for a New Critical Size. Phys. Chem. Chem. Phys. 2018; 20:802-818.
Coates RA, Armentrout PB. Thermochemical Investigations of Hydrated Nickel Dications Complexes by Threshold Collision-Induced Dissociation and Density Functional Theory. J. Phys. Chem. A 2017; 121:3629-3646.
Cooper TE, Armentrout PB. Experimental and Theoretical Investigation of the Charge-Separation Energies of Hydrated Zinc(II): Redefinition of the Critical Size. J. Phys. Chem. A 2009; 113:13742-13751.
Cooper TE, Armentrout PB. Sequential Bond Energies and Barrier Heights for the Water Loss and Charge Separation Dissociation Pathways of $Cd^{2+}(H_2O)_n$, n = 3-11. J. Chem. Phys. 2011; 134:114308.
Cooper TE, Armentrout PB. Threshold Collision-induced Dissociation of Hydrated Cadmium (II): Experimental and Theoretical Investigation of the Binding Energies for $Cd^{2+}(H_2O)_n$ Complexes (n = 4 – 11). Chem. Phys. Lett. 2010; 486:1-6.
Cooper TE, Carl DR, Armentrout PB. Hydration Energies of Zinc (II): Threshold Collision-induced Dissociation Experiments and Theoretical Studies. J. Phys. Chem. A 2009; 113:13727–13741.
Cooper TE, O'Brien JT, Williams ER, Armentrout PB. Zn^{2+} has a Primary Hydration Sphere of Five: IR Action Spectroscopy and Theoretical Studies of Hydrated Zn^{2+} Complexes. J. Phys. Chem. A 2010; 114:12646–12655.
Dalleska NF, Honma K, Armentrout PB. Stepwise Solvation Enthalpies of Protonated Water Clusters: Collision Induced Dissociation as an Alternative to Equilibrium Studies. J. Am. Chem. Soc. 1993; 115:12125-12131.
Dalleska NF, Honma K, Sunderlin LS, Armentrout PB. Solvation of Transition Metal Ions by Water. Sequential Binding Energies of $M^+(H_2O)_x$ (x = 1 - 4) for M = Ti - Cu Determined by Collision-Induced Dissociation. J. Am. Chem. Soc. 1994; 116:3519-3528.
Dalleska NF, Tjelta BL, Armentrout PB. Sequential Bond Energies of Water to Na^+ ($3s^0$), Mg^+($3s^1$), and Al^+ ($3s^2$). J. Phys. Chem. 1994; 98:4191-4195.
Daly NR. Scintillation Type Mass Spectrometer Ion Detector. Rev. Sci. Instrum. 1960; 31:264-267.
Ditchfield R, Hehre WJ, Pople JA. Self-Consistent Molecular-Orbital Methods. IX. An Extended Gaussian-Type Basis for Molecular-Orbital Studies of Organic Molecules. J. Chem. Phys. 1971; 54:724-728.
Donald WA, Leib RD, Demireva M, Negru B, Neumark DM, Williams ER. Average Sequential Water Molecule Binding Enthalpies of $M(H_2O)_{19\text{-}124}^{2+}$ (M = Co, Fe, Mn, and Cu) Measured with Ultraviolet Photodissociation at 193 and 248 nm. J. Phys. Chem. A 2011; 115:2-12.
Dzidic I, Kebarle P. Hydration of the alkali ions in the gas phase. Enthalpies and entropies of reactions $M^+(H_2O)_{n-1} + H_2O = M^+(H_2O)_n$. J. Phys. Chem. 1970; 74:1466-1474.
Ervin KM, Armentrout PB. Translational Energy Dependence of $Ar^+ + XY \rightarrow ArX^+ + Y$ (XY = H_2, D_2, HD) from Thermal to 30 eV c.m. J. Chem. Phys. 1985; 83:166-189.
Fergusson JE. 1990. The Heavy Elements: Chemistry, Environmental Impact, and Health Effects. Oxford Pergamon Press.

Foresman JB, Frisch AE. 1996. Exploring Chemistry with Electronic Structure Methods. Pittsburgh, PA: Gaussian, Inc.

Frisch MJ, Trucks GW, Schlegel HB, Scuseria GE, Robb MA, Cheeseman JR, Montgomery J, J. A. , Vreven T, Kudin KN, Burant JC, Millam JM, Iyengar SS, Tomasi J, Barone V, Mennucci B, Cossi M, Scalmani G, Rega N, Petersson GA, Nakatsuji H, Hada M, Ehara M, Toyota K, Fukuda R, Hasegawa J, Ishida M, Nakajima T, Honda Y, Kitao O, Nakai H, Klene M, Li X, Knox JE, Hratchian HP, Cross JB, Bakken V, Adamo C, Jaramillo J, Gomperts R, Stratmann RE, Yazyev O, Austin AJ, Cammi R, Pomelli C, Ochterski JW, Ayala PY, Morokuma K, Voth GA, Salvador P, Dannenberg JJ, Zakrzewski VG, Dapprich S, Daniels AD, Strain MC, Farkas O, Malick DK, Rabuck AD, Raghavachari K, Foresman JB, Ortiz JV, Cui Q, Baboul AG, Clifford S, Cioslowski J, Stefanov BB, Liu G, Liashenko A, Piskorz P, Komaromi I, Martin RL, Fox DJ, Keith T, Al-Laham MA, Peng CY, Nanayakkara A, Challacombe M, Gill PMW, Johnson B, Chen W, Wong MW, Gonzalez C, Pople JA. 2005. Gaussian 03, Revision D.01. Pittsburgh, PA: Gaussian, Inc.

Frisch MJ, Trucks GW, Schlegel HB, Scuseria GE, Robb MA, Cheeseman JR, Scalmani G, Barone V, Mennucci B, Petersson GA, Nakatsuji H, Caricato M, Li X, Hratchian HP, Izmaylov AF, Bloino J, Zheng G, Sonnenberg JL, Hada M, Ehara M, Toyota K, Fukuda R, Hasegawa J, Ishida M, Nakajima T, Honda Y, Kitao O, Nakai H, Vreven T, Montgomery JA, Peralta JE, Ogliaro F, Bearpark M, Heyd JJ, Brothers E, Kudin KN, Staroverov VN, Kobayashi R, Normand J, Raghavachari K, Rendell A, Burant JC, Millam JM, Iyengar SS, Tomasi J, Cossi M, Rega N, Millam JM, Klene M, Knox JE, Cross JB, Bakken V, Adamo C, Jaramillo J, Gomperts R, Stratmann RE, Yazyev O, Austin AJ, Cammi R, Pomelli C, Ochterski JW, Martin RL, Morokuma K, Zakrzewski VG, Voth GA, Salvador P, Dannenberg JJ, Dapprich S, Daniels AD, Farkas O, Foresman JB, Ortiz JV, Cioslowski J, Fox DJ. 2009. Gaussian 09, Revision A.02. Pittsburgh, PA: Gaussian Inc.

Frisch MJ, Trucks GW, Schlegel HB, Scuseria GE, Robb MA, Cheeseman JR, Scalmani G, Barone V, Mennucci B, Petersson GA, Nakatsuji H, Caricato M, Li X, Hratchian HP, Izmaylov AF, Bloino J, Zheng G, Sonnenberg JL, Hada M, Ehara M, Toyota K, Fukuda R, Hasegawa J, Ishida M, Nakajima T, Honda Y, Kitao O, Nakai H, Vreven T, Montgomery Jr. JA, Peralta JE, Ogliaro F, Bearpark MJ, Heyd J, Brothers EN, Kudin KN, Staroverov VN, Kobayashi R, Normand J, Raghavachari K, Rendell AP, Burant JC, Iyengar SS, Tomasi J, Cossi M, Rega N, Millam NJ, Klene M, Knox JE, Cross JB, Bakken V, Adamo C, Jaramillo J, Gomperts R, Stratmann RE, Yazyev O, Austin AJ, Cammi R, Pomelli C, Ochterski JW, Martin RL, Morokuma K, Zakrzewski VG, Voth GA, Salvador P, Dannenberg JJ, Dapprich S, Daniels AD, Farkas Ö, Foresman JB, Ortiz JV, Cioslowski J, Fox DJ. 2009. Gaussian 09, Revision D.01 Wallingford, CT, USA: Gaussian, Inc.

Frisch MJ, Trucks GW, Schlegel HB, Scuseria GE, Robb MA, Cheeseman JR, Scalmani G, Barone V, Petersson GA, Nakatsuji H, Li X, Caricato M, Marenich AV, Bloino J, Janesko BG, Gomperts R, Mennucci B, Hratchian HP, Ortiz JV, Izmaylov AF, Sonnenberg JL, Williams-Young D, Ding F, Lipparini F, Egidi F, Goings J, Peng B, Petrone A, Henderson T, Ranasinghe D, Zakrzewski VG, Gao J, Rega N, Zheng G, Liang W, Hada M, Ehara M, Toyota K, Fukuda R, Hasegawa J, Ishida M, Nakajima T, Honda Y, Kitao O, Nakai H, Vreven T, Throssell K, J. A. Montgomery J, Peralta JE, Ogliaro F, Bearpark MJ, Heyd JJ, Brothers EN, Kudin KN, Staroverov VN, Keith TA, Kobayashi R, Normand J, Raghavachari K, Rendell AP, Burant JC, Iyengar SS, Tomasi J, Cossi M, Millam JM, Klene M, Adamo C, Cammi R, Ochterski JW, Martin RL, Morokuma K, Farkas O, Foresman JB, Fox DJ. 2016. Gaussian 16, Revision A.03. Wallingford CT: Gaussian, Inc.

Gerlich D. Inhomogeneous rf Fields: A Versatile Tool for the Study of Processes with Slow Ions. Adv. Chem. Phys. 1992; 82:1-176.
Gilbert RG, Smith SC. 1990. Theory of Unimolecular and Recombination Reactions. London: Blackwell Scientific.
Glendening ED, Feller D. Dication−Water Interactions: $M^{2+}(H_2O)_n$ Clusters for Alkaline Earth Metals M = Mg, Ca, Sr, Ba, and Ra. J. Phys. Chem. 1996; 100:4790-4797.
Hales DA, Armentrout PB. Effect of Internal Excitation on the Collision-Induced Dissociation and Reactivity of Co_2^+. J. Cluster Science 1990; 1:127-142.
Hales DA, Lian L, Armentrout PB. Collision-Induced Dissociation of Nb_n^+ (n = 2 - 11): Bond Energies and Dissociation Pathways. Int. J. Mass Spectrom. Ion Processes 1990; 102:269-301.
Hofstetter TE, Armentrout PB. Threshold Collision-Induced Dissociation and Theoretical Studies of Hydrated Fe(II): Binding Energies and Coulombic Barrier Heights. J. Phys. Chem. A 2013; 117:1110-1123.
Holbrook KA, Pilling MJ, Robertson SH. 1996. Unimolecular Reactions. New York: Wiley.
Irving H, Williams RJP. 637. The stability of transition-metal complexes. Journal of the Chemical Society (Resumed) 1953:3192-3210.
Jayaweera P, Blades AT, Ikonomou MG, Kebarle P. Production and study in the gas phase of multiply charged solvated or coordinated metal ions. J. Am. Chem. Soc. 1990; 112:2452-2454.
Kafle A, Nwokolo C, Sanchez L, Armentrout PB. Threshold Collision-Induced Dissociation of Hydrated Thorium Trihydroxide Cation (IV): Experimental and Theoretical Investigation of the Binding Energies for $Th(OH)_3^+(H_2O)_n$ Complexes (n = 1 – 4). J. Phys. Chem. A 2020; 124:3090-3100.
Kaupp M, Schleyer PvR, Stoll H, Preuss H. Pseudopotential approaches to Ca, Sr, and Ba hydrides. Why are some alkaline earth MX2 compounds bent? J. Chem. Phys. 1991; 94:1360-1366.
Klobukowski M. Computational studies on hydrates of alkaline-earth dications. Can. J. Chem. 1992; 70:589-595.
Koizumi H, Larsen M, Muntean F, Armentrout PB. Sequential Bond Energies of $Ag^+(H_2O)_n$ and Ag^+(dimethyl ether)$_n$, n = 1 - 4, Determined by Threshold Collision-induced Dissociation. Int. J. Mass Spectrom. 2003; 228:221-235.
Moision RM, Armentrout PB. An Electrospray Ionization Source for Thermochemical Investigation with the Guided Ion Beam Mass Spectrometer. J. Am. Soc. Mass Spectrom. 2007; 18:1124-1134.
Möller C, Plesset MS. Note on an Approximation Treatment for Many-Electron Systems. Phys. Rev. 1934; 46:618-622.
Muntean F, Armentrout PB. Guided Ion Beam Study of Collision-Induced Dissociation Dynamics: Integral and Differential Cross Sections. J. Chem. Phys. 2001; 115:1213-1228.
O'Brien JT, Williams ER. Hydration of Gaseous Copper Dications Probed by IR Action Spectroscopy. J. Phys. Chem. A 2008; 112:5893-5901.
Peschke M, Blades AT, Kebarle P. Binding energies for doubly-charged ions M^{2+} = Mg^{2+}, Ca^{2+} and Zn^{2+} with the ligands L = H_2O, acetone and N-methylacetamide in complexes ML_n^{2+} for n = 1 - 7 from gas phase equilibra determinations and theoretical calculations. J. Am. Chem. Soc. 2000; 122:10440-10449.
Peschke M, Blades AT, Kebarle P. Formation, acidity and charge reduction of the hydrates of doubly charged ions M^{2+} (Be^{2+}, Mg^{2+}, Ca^{2+}, Zn^{2+}). Int. J. Mass Spectrom. 1999; 185/186/187:685–699.

Peschke M, Blades AT, Kebarle P. Hydration Energies and Entropies for Mg^{2+}, Ca^{2+}, Sr^{2+}, and Ba^{2+} from Gas-phase Ion-water Molecule Equilibria Determinations. J. Phys. Chem. A 1998; 102:9978-9985.

Rodgers MT, Armentrout PB. Collision-Induced Dissociation Measurements on $Li^+(H_2O)_n$, n = 1 - 6: The First Direct Measurement of the Li^+-OH_2 Bond Energy. J. Phys. Chem. A 1997; 101:1238-1249.

Rodgers MT, Armentrout PB. Statistical Modeling of Competitive Threshold Collision-Induced Dissociation. J. Chem. Phys. 1998; 109:1787-1800.

Rodgers MT, Ervin KM, Armentrout PB. Statistical Modeling of Collision-Induced Dissociation Thresholds. J. Chem. Phys. 1997; 106:4499-4508.

Rodriguez-Cruz SE, Jockusch RA, Williams ER. Binding Energies of Hexahydrated Alkaline Earth Metal Ions, $M^{2+}(H_2O)_6$, M = Mg, Ca, Sr, Ba: Evidence of Isomeric Structures for Magnesium. J. Am. Chem. Soc. 1999; 121:1986-1987.

Rodriguez-Cruz SE, Jockusch RA, Williams ER. Hydration Energies and Structures of Alkaline Earth Metal Ions, $M^{2+}(H_2O)_n$, n = 5-7, M = Mg, Ca, Sr, and Ba. J. Am. Chem. Soc. 1999; 121:8898-8906.

Rodriguez-Cruz SE, Jockusch RA, Williams ER. Hydration Energies of Divalent Metal Ions, $Ca^{2+}(H_2O)_n$ (n = 5-7) and $Ni^{2+}(H_2O)_n$ (n = 6-8), Obtained by Blackbody Infrared Radiative Dissociation. J. Am. Chem. Soc. 1998; 120:5842-5843.

Salomons W, Förstner U, Mader P. 1995. Heavy metals : problems and solutions. Berlin, New York: Springer-Verlag.

Sander O, Armentrout PB. Hydration Energies of Iron Hydroxide Cation: A Guided Ion Beam and Theoretical Investigation. J. Phys. Chem. A 2019; 123:1675-1688.

Schultz RH, Armentrout PB. Gas-Phase Metal Ligation: Collision-induced Dissociation of $Fe(H_2O)_x^+$ and $Fe(CH_4)_x^+$ (x = 1 - 4). J. Phys. Chem. 1993; 97:596-603.

Schultz RH, Armentrout PB. Threshold Collisional Activation of $Fe^+ \cdot C_3H_8$: Probing the Potential Energy Surface. J. Am. Chem. Soc. 1991; 113:729-730.

Searles SK, Kebarle P. Hydration of the Potassium Ion in the Gas Phase: Enthalpies and Entropies of Hydration Reactions $K^+(H_2O)_{n-1} + H_2O = K^+(H_2O)_n$ for n = 1 to n = 6. Can. J. Chem. 1969; 47:2619-2627.

Shaffer SA, Prior DC, Anderson GA, Udseth HR, Smith RD. An Ion Funnel Interface for Improved Ion Focusing and Sensitivity Using Electrospray Ionization Mass Spectrometry. Anal. Chem. 1998; 70:4111-4119.

Shannon RD. Revised Effective Ionic Radii and Systematic Studies of Interatomic Distances in Halides and Chalcogenides. Acta Cryst. 1976; A32:751-767.

Shvartsburg AA, Siu KWM. Is There a Minimum Size for Aqueous Doubly Charged Metal Cations? J. Am. Chem. Soc. 2001; 123:10071-10075.

Stein SE, Rabinovich BS. On the Use of Exact State Counting Methods in RRKM Rate Calculations. Chem. Phys. Lett. 1977; 49:183-188.

Stein SE, Rabinovitch BS. Accurate Evaluation of Internal Energy Level Sums and Densities Including Anharmonic Oscillators and Hindered Rotors. J. Chem. Phys. 1973; 58:2438-2445.

Stone JA, Vukomanovic D. Collisional dissociation studies of $Cu^{2+}(H_2O)_n$ using electrospray ionization mass spectrometry. Int. J. Mass Spectrom. 1999; 185–187:227-229.

Sweeney AF, Armentrout PB. Guided Ion Beam Studies of the Collision-induced Dissociation of $CuOH^+(H_2O)_n$ (n = 1-4): Comprehensive Thermodynamic Data for Copper Ion Hydration. J. Phys. Chem. A 2014; 118:10210-10222.

Sweeney AF, Armentrout PB. Hydrated Copper Ion Chemistry: Guided Ion Beam and Computational Investigation of $Cu^{2+}(H_2O)_n$ (n = 7 – 10) Complexes. Eur. J. Mass Spectrom. 2015; 21:497-516.

Truhlar DG, Garrett BC, Klippenstein SJ. Current Status of Transition-State Theory. J. Phys. Chem. 1996; 100:12771-12800.

van Duijneveldt FB, van Duijneveldt-van de Rijdt JGCM, van Lenthe JH. State of the Art in Counterpoise Theory. Chem. Rev. 1994; 94:1873-1885.

Weigend F, Ahlrichs R. Balanced basis sets of split valence, triple zeta valence and quadruple zeta valence quality for H to Rn: Design and assessment of accuracy. Phys. Chem. Chem. Phys. 2005; 7:3297-3305.

Wheeler OW, Carl DR, Armentrout PB. Second–Shell Thermochemistry for Hydration of Strontium Dications as Determined by Threshold Collision-Induced Dissociation and Computations. Int. J. Mass Spectrom. 2018; 429:76-89.

Wheeler OW, Carl DR, Hofstetter TE, Armentrout PB. Hydration Enthalpies of $Ba^{2+}(H_2O)_x$, x = 1 – 8: A Threshold Collision-Induced Dissociation and Computational Investigation. J. Phys. Chem. A 2015; 119:3800-3815.

Wong RL, Paech K, Williams ER. Blackbody Infrared Radiative Dissociation at Low Temperature Hydration of $X^{2+}(H_2O)_n$, for X = Mg, Ca Int. J. Mass Spectrom. 2004; 232:59-66.

Yang F, Coates R, Boles GC, Armentrout PB. Thermochemical Studies of Hydrated Manganese Dications, $Mn^{2+}(H_2O)_x$ (x = 4 – 10) Using Guided Ion Beam Tandem Mass Spectrometry. Int. J. Mass Spectrom. 2021; 468:116638.

Ye SJ, Armentrout PB. Absolute Thermodynamic Measurements of Alkali Metal Cation Interactions with a Simple Dipeptide and Tripeptide. J. Phys. Chem. A 2008; 112:3587-3596.

Table 1. Hydration energies (kJ/mol) at 0 K of alkaline earth metal dications, $M^{2+}(H_2O)_x$, determined using TCID compared to BIRD and HPMS values. Uncertainties in parentheses.

M^{2+}	x	TCID [a]		BIRD [b]		HPMS [c]	
Mg^{2+}	2	256	(36)				
	3	226	(15)				
	4	178	(10)				
	5	116	(9)	107	(5)		
	6	97	(8)	98	(7)	100	(4)
	7	70	(8)	75	(5)	82	(4)
	8	67	(7)	75	(8)	71	(4)
	9	59	(7)	67	(6)	67	(4)
	10	44	(6)	52	(4)	65	(4)
Ca^{2+}	1	243	(6)				
	2	197	(17)				
	3	170	(9)				
	4	141	(9)				
	5	112	(8)	110	(6)		
	6	99	(9)	90	(3)	104	(4)
	7	59	(11)	70	(5)	67	(4)
	8	57	(12)	69	(6)	63	(4)
	9	58	(3)	61	(6)	60	(4)
Sr^{2+}	1	201	(6)				
	2	172	(5)				
	3	144	(5)				
	4	124	(4)				
	5	103	(4)	100	(4)		

	6	94	(3)	86	(4)	94	(4)
	7	59	(5)	70	(4)	67	(4)
	8	52	(6)			63	(4)
	9	53	(6)			61	(4)
Ba^{2+}	1	169	(5)				
	2	145	(7)				
	3	129	(4)				
	4	107	(4)	107	(4)		
	5	92	(6)	88	(3)	99	(4)
	6	77	(5)	75	(3)	82	(4)
	7	55	(6)	64	(3)	66	(4)
	8	48	(9)			61	(4)

[a] (Carl & Armentrout, 2012;Carl & Armentrout, 2013;Carl, et al., 2010;Carl, et al., 2007;Wheeler, et al., 2018;Wheeler, et al., 2015).

[b] (Rodriguez-Cruz, et al., 1999;Rodriguez-Cruz, et al., 1999;Wong, et al., 2004)

[c] (Peschke, et al., 1998)

Table 2. M^{2+} ionic radii and M-O bond lengths (Å) for ground structures of $M^{2+}(H_2O)_x$ where M is a Group 2 metal predicted by MP2(full)//B3LYP calculations where all water ligands are in the inner solvent shell. Degeneracies in parentheses.

M^{2+}	Ionic Radius [a]	x = 1	2		3		4		5		6		7		8	
Mg^{2+}	0.72	1.942	1.958	(2)	1.987	(3)	2.021	(4)	2.050	(2)	2.113	(6)				
									2.060							
									2.105	(2)						
Ca^{2+}	1.00	2.244	2.282	(2)	2.313	(3)	2.340	(4)	2.364		2.405	(6)				
									2.365	(2)						
									2.393	(2)						
Sr^{2+}	1.18	2.418	2.455	(2)	2.487	(3)	2.517	(4)	2.538		2.582	(6)	2.595	(2)		
									2.543	(2)			2.614			
									2.568	(2)			2.619	(2)		
													2.639	(2)		
Ba^{2+}	1.35	2.602	2.647	(2)	2.680	(3)	2.712	(4)	2.737		2.784	(6)	2.796	(2)	2.839	(3)
									2.743	(2)			2.810	(2)	2.840	(5)
									2.765	(2)			2.813			
													2.827	(2)		

[a] (Shannon, 1976).

Table 3**.** Hydration energies (kJ/mol) at 0 K of late first-row transition metal and Cd dications, $M^{2+}(H_2O)_x$, determined using TCID. Uncertainties are in parentheses.

x	Mn		Fe		Co		Ni		Cu		Zn		Cd	
3	205	(3)											186	(14)
4	171	(6)	167	(12)	168	(8)	156	(9)					147	(4)
5	108	(7)	108	(6)	100	(6)	128	(5)					107	(5)
6	88	(5)	95	(6)	107	(7)	113	(7)			95	(4)	87	(5)
7	72	(4)	78	(5)	77	(8)	83	(6)	101	(3)	79	(5)	68	(5)
8	72	(4)	69	(7)	68	(6)	69	(9)	73	(4)	68	(6)	64	(6)
9	68	(4)	55	(4)	58	(7)	49	(6)	50	(6)	53	(8)	59	(5)
10			50	(6)	46	(7)	46	(3)	38	(6)	43	(3)	47	(5)
11			46	(3)	40	(7)	40	(4)					42	(5)

Table 4. M^{2+} ionic radii and bond lengths (Å) of ground structures of $M^{2+}(H_2O)_x$ where M is a late first-row transition metals for complexes with all water ligands in the inner solvent shell as determined by MP2/6-311+G(2d,2p)//B3LYP/6-311+G(d,p) calculations. Degeneracies in parentheses.

M^{2+}	Ionic Radius[a]	$x = 1$	2		3		4		5		6	
Mn^{2+}	0.83	1.985	1.998	(2)	2.060	(3)	2.108	(4)	2.149	(2)	2.217	(6)
									2.150			
									2.201	(2)		
Fe^{2+}	0.78	1.927	1.972	(2)	2.000	(3)	2.046	(4)	2.075	(2)	2.143	(2)
									2.129		2.167	(2)
									2.143	(2)	2.181	(2)
Co^{2+}	0.74	1.884	1.901	(2)	1.955		2.012	(4)	1.998	(2)	2.001	(6)
					1.956	(2)			2.013	(2)		
									3.686			
Ni^{2+}	0.69	1.875	1.870	(2)	1.898	(3)	1.999	(4)	2.025	(2)	2.087	(6)
									2.034			
									2.073	(2)		
Cu^{2+}	0.73						1.982	(4)	1.986	(2)	1.965	(4)
									2.025		3.733	(2)
									2.196	(2)		

Zn^{2+}	0.74	1.881	1.876	(2)	1.944	(2)	2.002	(4)	2.038	(2)	2.128	(6)
					1.953				2.055			
									2.127	(2)		

[a] Six-coordinate values. High spin for Mn^{2+}, Fe^{2+}, and Co^{2+}. Values taken from ref. (Shannon, 1976).

Table 5. Critical sizes for dissociative charge transfer in $M^{2+}(H_2O)_x$ and the second ionization energy (IE) of M.

M	Second IE (eV)[a]	Critical Sizes Kebarle et al. [b]	Shvartzburg and Siu [c]	TCID	CS chan.[d]
Ba	10.00	0	2	3	0+2
Sr	11.03	2	2	2	0+1
Ca	11.87	2	2	3	0+1, 1+1
Mg	15.04	3	4	4	1+1, 2+1
Mn	15.64	3	4	4	1+1, 2+1, 2+2
Fe	16.20	5	5	4	2+1, 2+2, 3+2, 3+3, 4+3
Cd	16.91		4	4	1+1, 2+1, 2+2
Co	17.08	4	5	6	2+1, 3+2, 3+3
Zn	17.96	5	6	7	3+3, 4+3
Ni	18.17	4	5	4	2+1, 2+2, 3+2
Cu	20.29	6[e]	6	8	3+3, 4+3

[a] NIST Atomic Spectra Database (2006). [b] Except as noted: (Blades, et al., 1990;Blades, et al., 1990;Jayaweera, et al., 1990;Peschke, et al., 1999). [c] (Shvartsburg & Siu, 2001).

[d] Charge separation channels observed in TCID experiments, where $y+(x-y-1)$ indicates formation of $MOH^+(H_2O)_y + H^+(H_2O)_{x-y-1}$ from $M^{2+}(H_2O)_x$ in reaction (2). [e] (Stone & Vukomanovic, 1999).

Figure Captions

Figure 1. Hydration energies at 0 K of Group 2 dications obtained using TCID.

Figure 2. 0 K hydration energies of Group 2 metal dications obtained using TCID plotted versus the M-O bond distances predicted for ground geometries using MP2(full)/6-311G+(2d,2p)//B3LYP/6-311+G(d,p).

Figure 3. Ground structures of $M^{2+}(H_2O)_x$ complexes of Mg and Sr with one to eight water molecules calculated at the MP2(full)//B3LYP level of theory.

Figure 4. Hydration energies at 0 K of late 3d transition metal dications obtained using TCID. The line represents the 0 K hydration energies of $Mg^{2+}(H_2O)_x$.

Figure 5. Ground structures of $Cu^{2+}(H_2O)_x$ complexes with seven and eight water molecules calculated at the MP2(full)//B3LYP level of theory.

Figure 6. Hydration energies at 0 K of Zn^{2+} and Cd^{2+} obtained using TCID. The line represents the 0 K hydration energies of $Mg^{2+}(H_2O)_x$.

Figure 7. High pressure (0.19 mTorr of Xe) cross sections for the TCID of $Ba^{2+}(H_2O)_3$. The primary water loss channel, $Ba^{2+}(H_2O)_2$, is represented by circles, secondary water loss channel. $Ba^{2+}(H_2O)$. is represented by upward triangles, and the tertiary channel, Ba^{2+}, is represented by squares. Downward triangles are the competing charge separation products, $BaOH^+$. Solid lines are the best fits to the cross sections of the product channels convoluted over the neutral and ion kinetic and internal energy distributions. The dashed lines show the models in the absence of

experimental kinetic energy broadening for the reactants with an internal energy at 0 K. Reproduced from (Wheeler, et al., 2015) with permission.

Figure 8. Reaction coordinates and structures for water loss (in red) and two charge separation pathways (in blue) of $Ba^{2+}(H_2O)_3$. Energies (kJ/mol) were calculated at the B3LYP/def2-TZVPP level of theory and include zero-point energies. Reproduced from (Wheeler, et al., 2015) with permission.

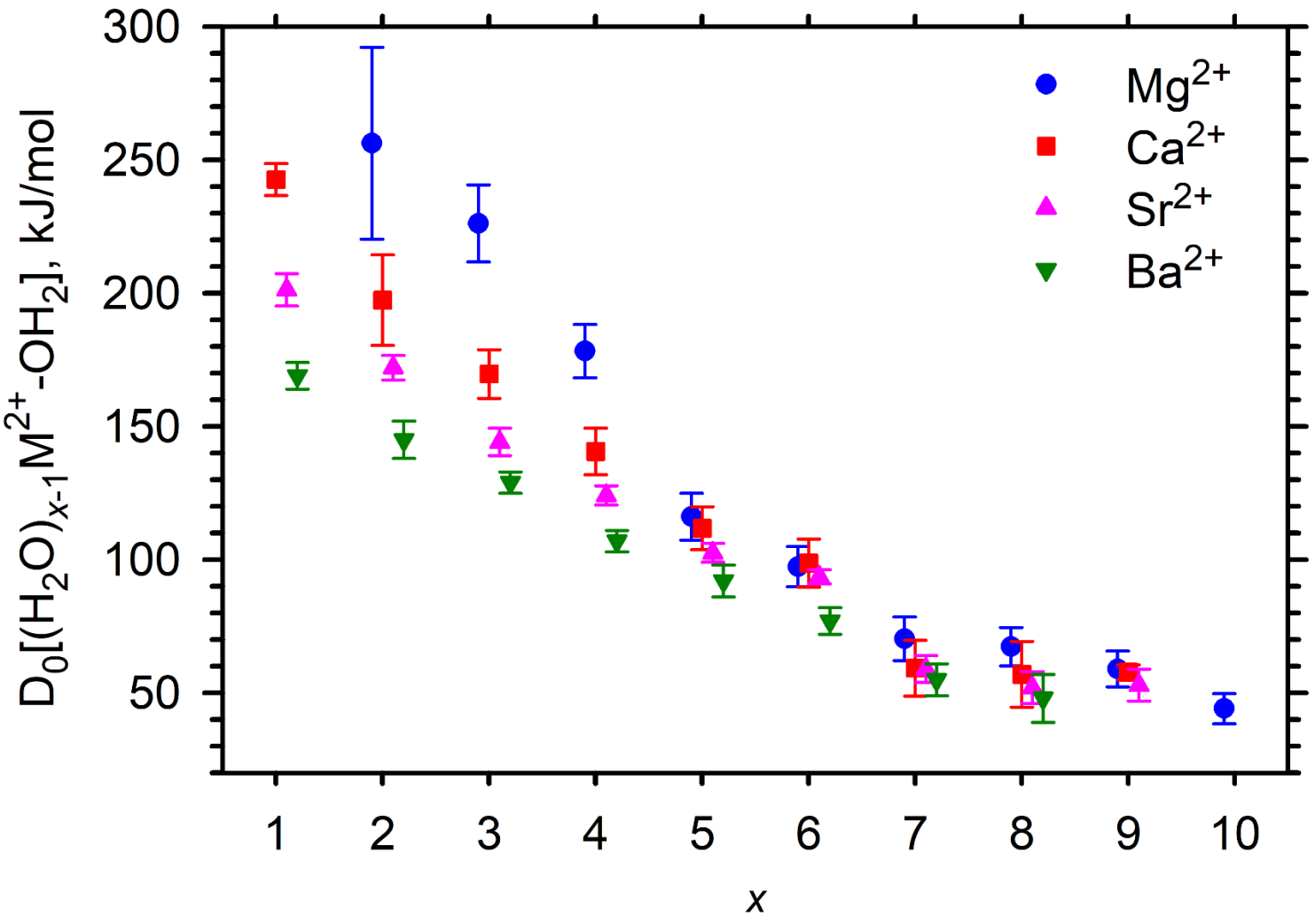
300
250
200
150
100
50
1
2
3
4
5
6
7
8
9
10
x
D0[(H2O)x-1M2+-OH2], kJ/mol
Mg2+
Ca2+
Sr2+
Ba2+

Figure 1

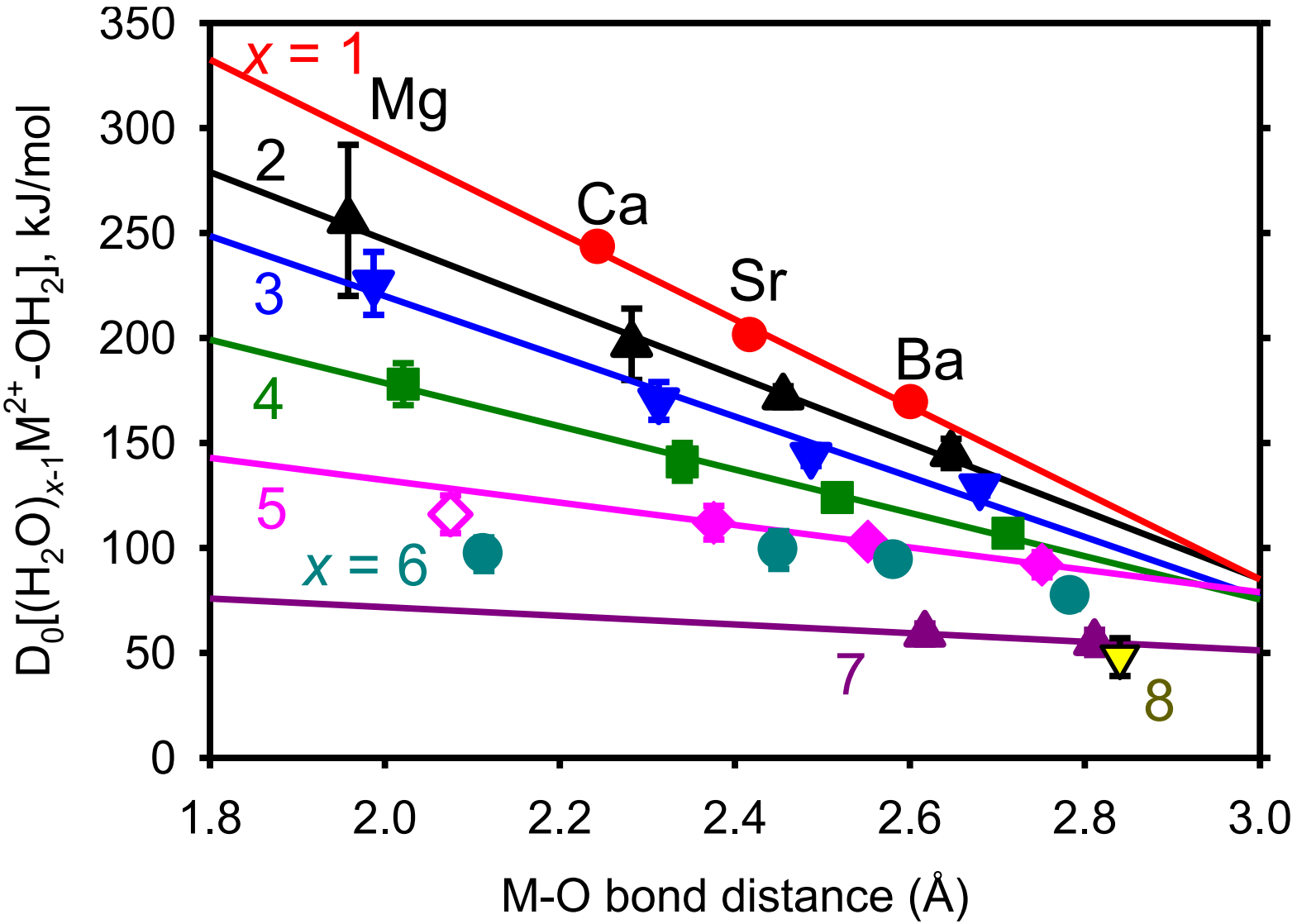
350
300
250
200
150
100
50
0
1.8
2.0
2.2
2.4
2.6
2.8
3.0
M-O bond distance (Å)
D0[(H2O)x-1M2+-OH2], kJ/mol
x = 1
Mg
2
Ca
Sr
Ba
3
4
5
x = 6
7
8

Figure 2

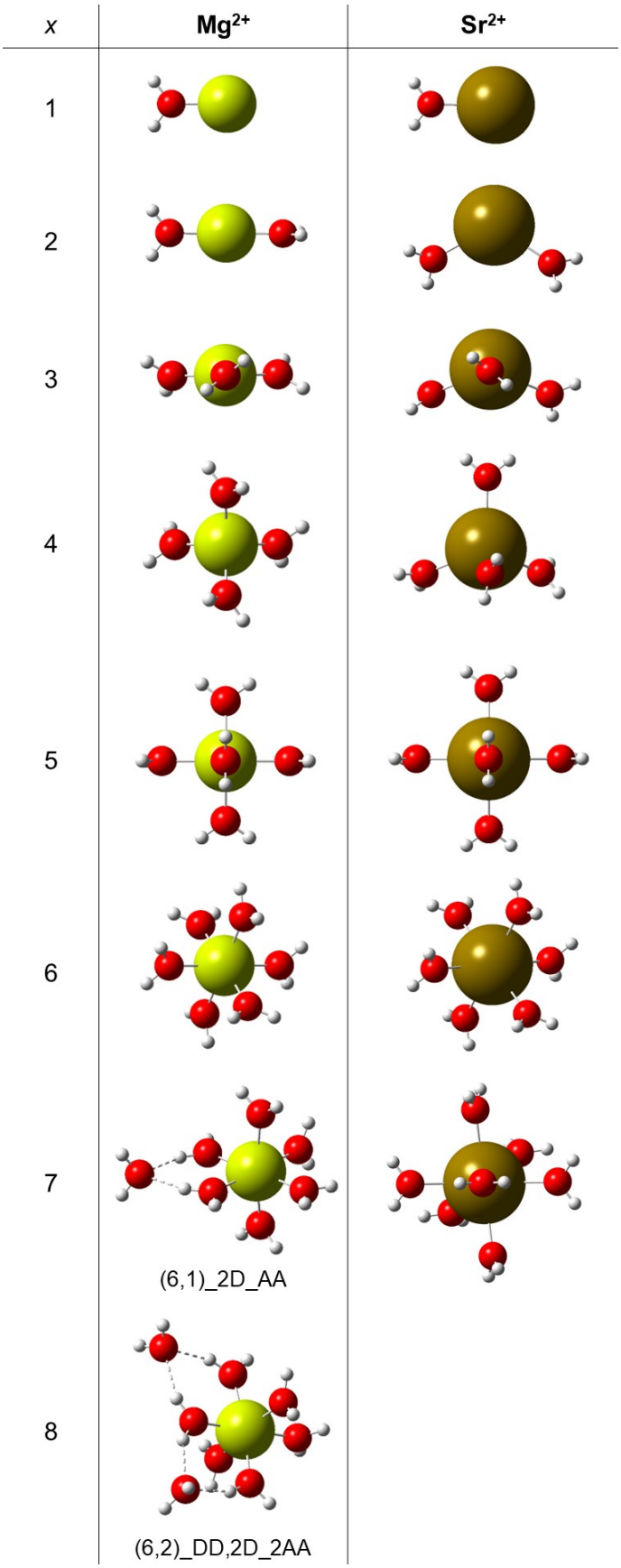

Figure 3

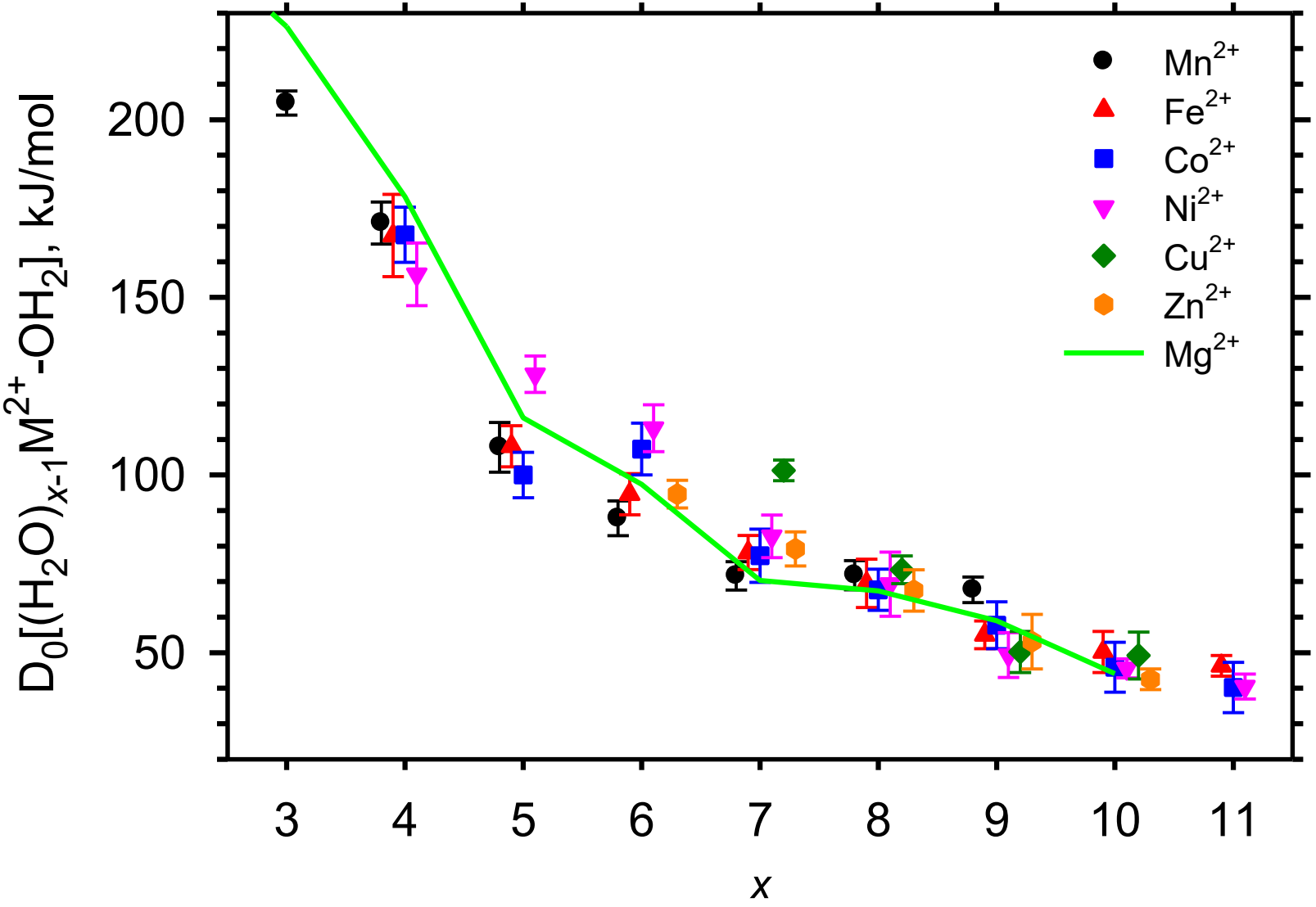
$D_0[(H_2O)_{x-1}M^{2+}\text{-}OH_2]$, kJ/mol
200
150
100
50
3
4
5
6
7
8
9
10
11
x
Mn^{2+}
Fe^{2+}
Co^{2+}
Ni^{2+}
Cu^{2+}
Zn^{2+}
Mg^{2+}

Figure 4

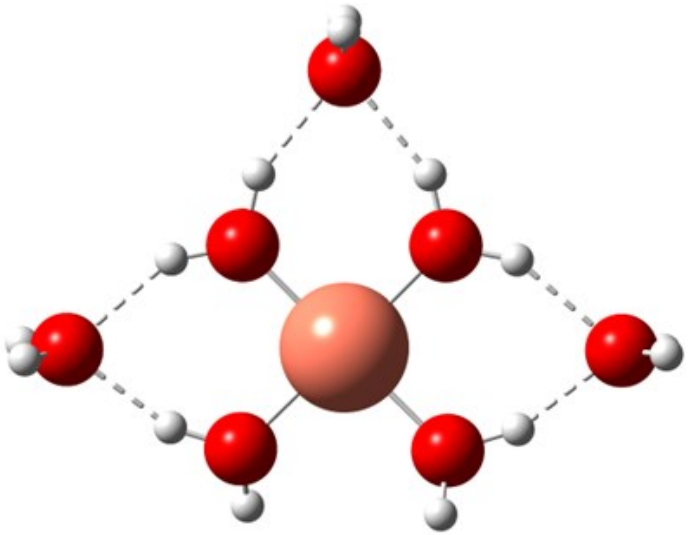

(4,3)_2DD,2D_3AA

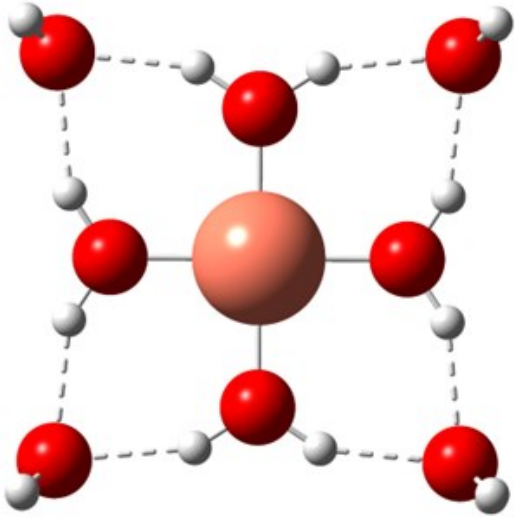

(4,4)_4DD_4AA

Figure 5

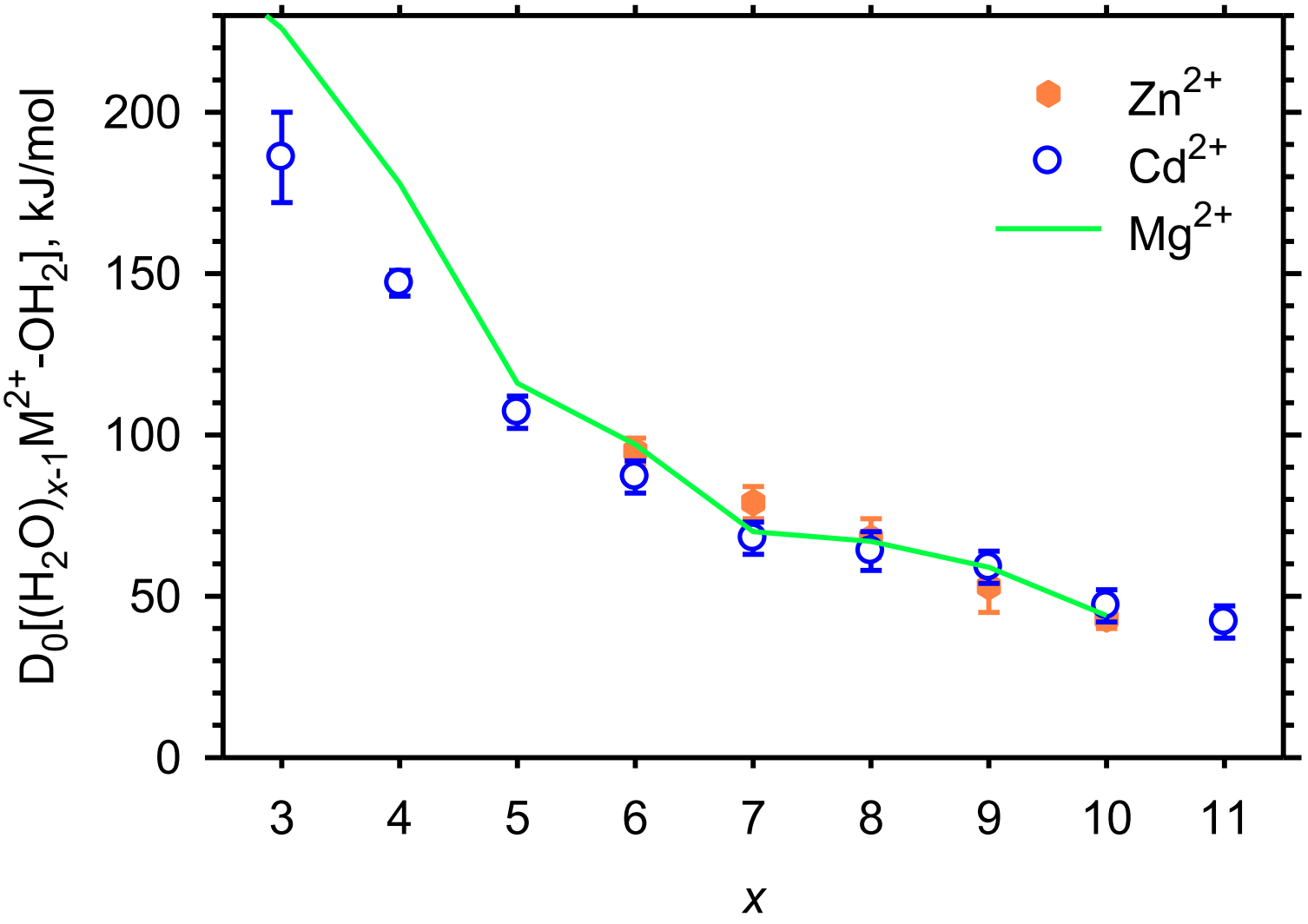
$D_0[(H_2O)_{x-1}M^{2+}\text{-}OH_2]$, kJ/mol
200
150
100
50
0
3
4
5
6
7
8
9
10
11
x
Zn^{2+}
Cd^{2+}
Mg^{2+}

Figure 6

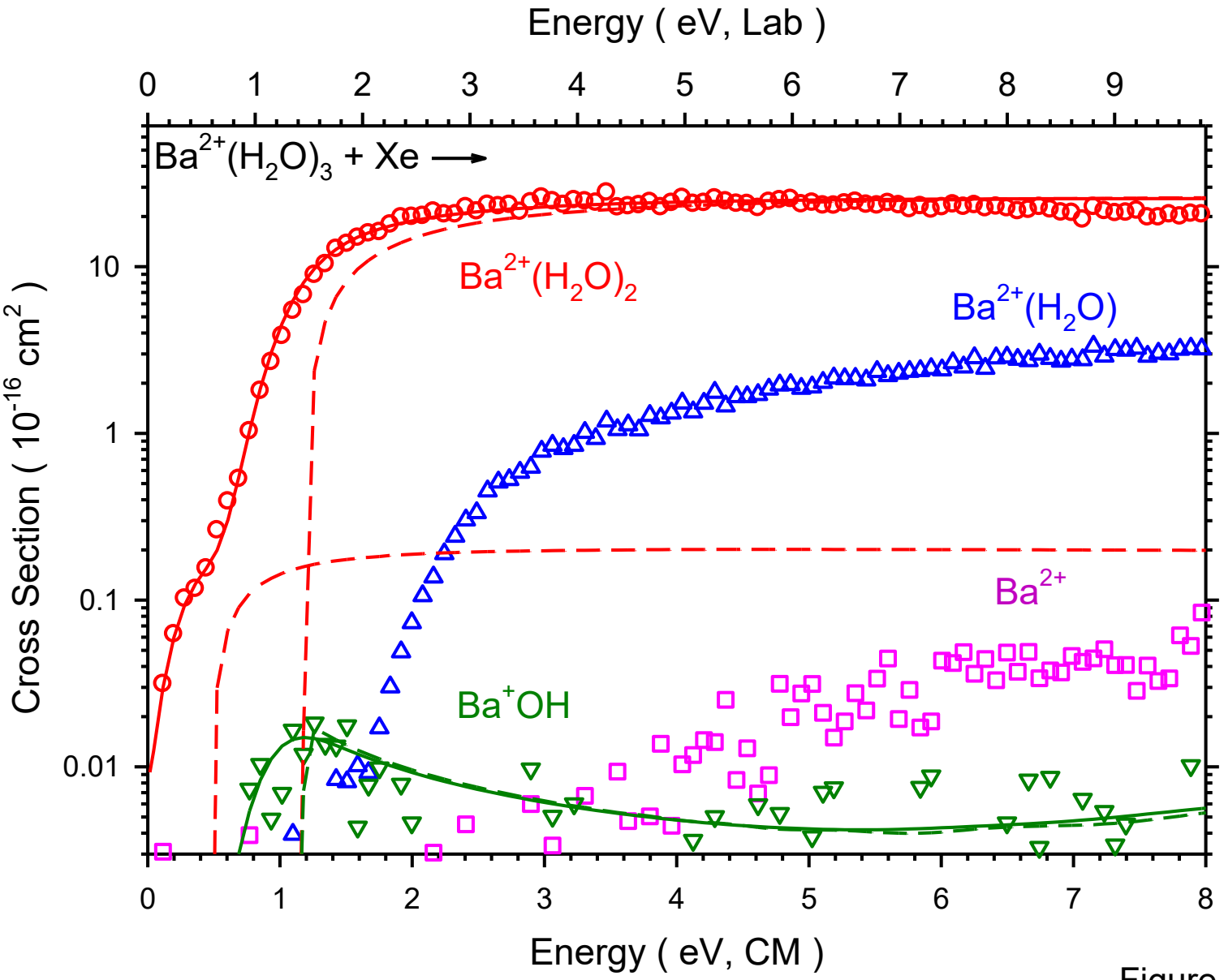
Energy (eV, Lab)
0
1
2
3
4
5
6
7
8
9
Ba2+(H2O)3 + Xe ⟶
Ba2+(H2O)2
Ba2+(H2O)
Ba2+
Ba+OH
Cross Section (10-16 cm2)
10
1
0.1
0.01
0
1
2
3
4
5
6
7
8
Energy (eV, CM)

Figure 7

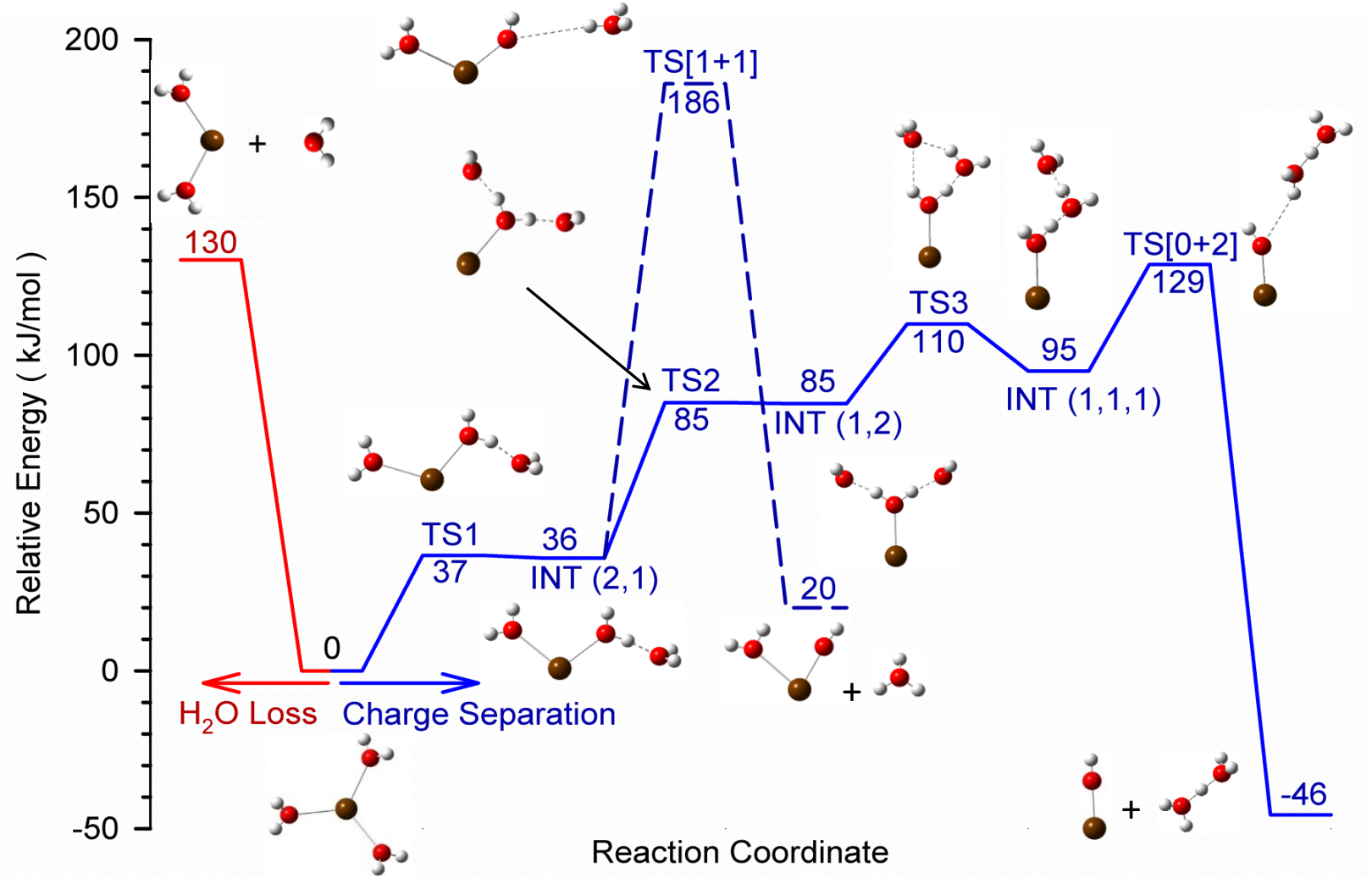
200
150
100
50
0
-50
Relative Energy (kJ/mol)
130
0
TS1
37
36
INT (2,1)
TS2
85
TS[1+1]
186
85
INT (1,2)
20
TS3
110
95
INT (1,1,1)
TS[0+2]
129
-46
H2O Loss
Charge Separation
Reaction Coordinate

Figure 8

Biographical sketches

Fan Yang: Fan Yang received a bachelor's degree in chemistry from Brigham Young University-Idaho in 2016. She is presently a physical chemistry Ph.D. candidate at the University of Utah working with Professor Peter B. Armentrout. Her graduate work has focused on measuring hydration energies of various metal dications and metal hydroxide ions using threshold collision-induced dissociation.

Peter B. Armentrout:

Henry Eyring Presidential Endowed Chair and Distinguished Professor, Department of Chemistry, University of Utah, Utah, USA

Some 40 years ago, Professor Armentrout and his group developed the first guided ion beam tandem mass spectrometer to quantitatively examine the kinetic energy dependence of ion–molecule reactions. In the interim, he and his group have developed sophisticated tools for analyzing the resultant reaction cross sections and thereby providing thermodynamic, kinetic, and dynamic information on a wide range of chemical species. Innovative use of a variety of ion sources has extended the applicability of these methods to a host of interesting inorganic and biological molecules. His group is well-known for providing quality thermodynamic information for species ranging from diatomic molecules to atomic clusters, to biopolymers, to the solvated systems discussed here. Professor Armentrout has been a faculty member in the Department of Chemistry at the University of Utah since 1987. He has been recognized by a number of awards and his research is documented in over 560 refereed articles and book chapters.